A&A 518, A64 (2010)
DOI: 10.1051/0004-6361/201014170

Astronomy & Astrophysics

R-matrix electron-impact excitation data for the Ne-like iso-electronic sequence⋆

G. Y. Liang and N. R. Badnell

Department of Physics, University of Strathclyde, Glasgow, G4 0NG, UK
e-mail: guiyun.liang@strath.ac.uk

Received 1 February 2010 / Accepted 7 May 2010

ABSTRACT

We present results for the electron-impact excitation of all Ne-like ions from Na^{+} to Kr^{26+} obtained using the intermediate-coupling frame transformation *R*-matrix approach. For each ion's calculation, the close-coupling expansion is taken to be the 113 LS terms (209 levels) belonging to the configurations $[1s^2]2s^22p^6$, $2s^22p^5\{3,4,5\}l$, $2s2p^6\{3,4,5\}l$ ($l \in$ s, p, d, f, and g), and $2s^22p^5\{6,7\}l'$ ($l' \in$ s, p, and d). An additional configuration interaction effect arising from configurations of $2s^22p^43l\{3,4,5\}l''$ ($l'' \in$ s, p, d, f and g) was included in the target expansion. A detailed comparison of the target structure has been made for six specific ions (Si^{4+}, Ar^{8+}, Ca^{10+}, Fe^{16+}, Ni^{18+}, and Kr^{26+}) spanning the sequence to assess the accuracy for the entire sequence. Effective collision strengths (Υs) are presented at temperatures ranging from $2\times10^2(q+1)^2$ K to $2\times10^6(q+1)^2$ K (where q is the residual charge of ions, i.e. $Z-10$). Detailed comparisons for the Υs are made with the results of previous calculations for several ions, which span the sequence. Furthermore, we examine the iso-electronic trends of effective collision strengths as a function of temperature. The present results are the only *R*-matrix ones for the majority of the ions and the most extensive and complete data for modelling to-date.

Key words. atomic data – atomic processes – plasmas

1. Introduction

Because Ne-like ions have a stable closed L-shell ground state, they show high abundance over a wide range of temperatures in ionization equilibrium for each iso-nuclear sequence (see Mazzotta et al. 1998; Bryans et al. 2006, 2009). Thus, they attract extensive studies for spectral diagnostic and modelling in astrophysical and laboratory plasmas, and in particular iron, due to its high cosmic abundance. X-ray lasers (Mathews et al. 1985; Tomasel et al. 1997) based on Ne-like ions are another significant area of interest. However, the atomic structure and electron-impact excitation (EIE) of Ne-like ions are extremely complex, which results in there being large uncertainties in line intensity ratios ($2p^53d\ ^1P_1 \rightarrow 2p^6\ ^1S_0$ vs $2p^53d\ ^3D_1 \rightarrow 2p^6\ ^1S_0$, this is usually designated $3C/3D$, as well as 3s – 2p vs. $3C$) between measurements or observations and predictions (Beiersdorfer et al. 2001, 2002; Gu et al. 2004). For example, even for iron, EIE of this ion has been investigated experimentally and theoretically for a long time (Smith et al. 1985; Chen et al. 2003; Loch et al. 2006; Beiersdorfer et al. 2001, 2002 and references therein).

Resonances in electron-ion impact excitation have been observed in laboratory measurements (Brown et al. 2006). They play an important role in the spectral diagnostic and modelling of astrophysical and laboratory plasmas. The close-coupling (CC) approximation (e.g. *R*-matrix, Hummer et al. 1993) satisfactorily reproduces and describes such resonances. Recently, there have been several works using this method for three ions in this iso-electronic sequence. Chen et al. (2003) performed (BPRM) Breit-Pauli *R*-matrix (Berrington et al. 1995) calculations for Fe^{16+} with an 89 fine-structure level close-coupling expansion (to $n = 4$). Loch et al. (2006) performed a fully-relativistic larger scale Fe^{16+} calculation (139 fine-structure levels, including an additional 50 levels of the $2p^55l$ configurations) using the Dirac atomic *R*-matrix code (DARC, Norrington & Grant 1987). Collisional-radiative (CR) modelling with their updated excitation data was also undertaken (Chen 2008; Loch et al. 2006), the combination of which gives satisfactory agreement between measurements/observations and theory for the $3C/3D$ line ratio. A benchmark work performed by Del Zanna & Ishikawa (2009) revealed the data of Loch et al. (2006) to be reliable. Similar differences for other (non-iron) ions in this iso-electronic sequence have been observed between measurements (Beiersdorfer et al. 2001) and theoretical predictions based upon distorted-wave (DW) excitation data. By making a semi-empirical configuration-interaction (CI) correction to excitation data and taking CR effects into account, Fournier & Hansen (2005) brought the predictions into agreement with measurements for Ne-like ions from Cr^{14+} to Ag^{37+}. This confirms again that accurate atomic data is essential for the reliable diagnostic modelling of astrophysical and laboratory plasmas. However, most excitation data in this iso-electronic sequence are from the DW approximation (Zhang et al. 1987; Bhatia et al. 1985), except for *R*-matrix calculations for three ions, viz Fe^{16+} (BPRM and DARC, as noted above), Ni^{18+}, and Kr^{26+} (both DARC). For Ni^{18+}, Aggarwal & Keenan (2008) performed an 89-level CC

⋆ These data are made available in the archives of APAP via http://www.apap-network.org, OPEN-ADAS via http://open.adas.ac.uk as well as anonymous ftp to cdsarc.u-strasbg.fr (130.79.128.5) or via
http://cdsweb.u-strasbg.fr/cgi-bin/qcat?J/A+A/518/A64

(n = 4, [1s^2]2s^{2}2p^6, 2s^{2}2p^5{3, 4}l, and 2s2p^6{3, 4}l) calculation and Chen et al. (2006) a 125-level ([1s^2]2s^{2}2p^6, 2s^{2}2p^5{3, 4, 5}l, and 2s2p^{6}3l) CC calculation. For Kr^{26+}, Griffin et al. (2008) used a 139-level (n = 5, [1s^2]2s^{2}2p^6, 2s^{2}2p^5{3, 4, 5}l, 2s2p^6{3, 4}l) CC expansion; they also demonstrated that the radiative damping of resonance contributions is a small effect.

Due to the advantage of high accuracy – see Griffin et al. (1998), Badnell & Griffin (1999), Berrington et al. (2005) and Liang et al. (2008) – and computational efficiency of the intermediate-coupling frame transformation (ICFT) R-matrix methodology and associated codes, along with the high capability of parallel computer clusters, it is now feasible to provide excitation data for iso-electronic sequences across the entire range of astrophysical interest within the R-matrix framework. Witthoeft et al. (2007) investigated the physics of electron-impact excitation along the F-like iso-electronic sequence (Ne$^+$ to Kr^{27+}) and Liang et al. (2009a,b) also did an entire sequence calculation for Na-like ions (for both outer- and inner-shell excitations) with Auger- and radiative-damping included for the inner-shell excitations. Based upon the robustness of the current suite of R-matrix codes, the R-matrix calculation of effective collision strengths (Υ) currently can be performed automatically for each ion without manual intervention along an iso-electronic sequence after sufficiently accurate radial wave functions have been obtained and CI/CC expansions have been confirmed. This ensures that each calculation is performed uniformly and reliably, as well as that the calculation along the sequence is consistent. Careful analysis of the results for several specified ions spanning the sequence is still necessary so as to further validate the accuracy of the data along the sequence.

In this paper, we report on the electron-impact excitation of the Ne-like iso-electronic sequence (from Na$^+$ to Kr^{26+}), via the ICFT R-matrix approach. In Sect. 2, we discuss details of the calculation method and pay particular attention on comparing our underlying atomic structure with previous results. The excitation results themselves are discussed in Sect. 3. Our work is a part of ongoing collaborative work – the UK Atomic Processes for Astrophysical Plasmas (APAP) network[1], a broadening of scope of the original UK RmaX network.

2. Sequence calculation

The aim of this work is to perform R-matrix calculations employing the ICFT method (see Griffin et al. 1998) for all Ne-like ions from Na$^+$ to Kr^{26+}. In our calculations we included the following 31 configuration basis set in our close-coupling expansion: [1s^2]2s^{2}2p^6, 2s^{2}2p^5{3, 4, 5}l, 2s2p^6{3, 4, 5}l ($l \in$ s, p, d, f and g) and 2s^{2}2p^5{6, 7}l' ($l' \in$ s, p and d), and an additional 33 correlation configuration – 2s^{2}2p^{4}3l{3, 4, 5}l' (l and $l' \in$ s, p, d, f and g) in our CI expansion. This results in 113 close-coupling LS terms and 209 fine-structure levels. The CI expansion consists of 1337 LS terms and 2775 fine-structure levels, which were determined to be important for improving the accuracy of the energy levels which we included in the close-coupling expansion.

2.1. Structure: energies

The target wave functions (1s-7d) were obtained from AUTOSTRUCTURE (AS, Badnell 1986) using the Thomas-Fermi-Dirac-Amaldi model potential. Relativistic effects were included perturbatively via the one-body Breit-Pauli operator (viz. mass-velocity, spin-orbit and Darwin) without valence electron two-body fine-structure operators. This is consistent with the operators included in the standard Breit-Pauli R-matrix suite of codes. The radial scaling parameters, λ_{nl} (n = 2 and 3; $l \in$ s, p and d), were obtained separately for each ion by a two-step optimization procedure with $\lambda_{\{1,4,5,6,7\}l}$ = 1.00. In the first step, the energy of the ground level 2s^{2}2p^6 ^{1}S$_0$ was minimized by varying the λ_{2s} and λ_{2p} scaling parameters. Then, the average-energy of the fine-structure levels of the 14 terms of the 2s^{2}2p^{5}3l configuration was minimized by varying the λ_{3l} scaling parameters. This optimization procedure was found to be the best common one that could be used for all ions over the sequence. Optimizing the nl (n = 4, 5, 6 and 7) orbitals was found to give only a small improvement of the target level energies for several specified ions (Si^{4+}, Fe^{16+} and Kr^{26+}) spanning the sequence. In order to maintain consistency and so as not to introduce arbitrary changes along the sequence, the optimization procedure is done automatically in AUTOSTRUCTURE without any manual re-adjustment. The resultant scaling parameters are listed in Table 1.

Table 1. Radial scaling factors used in AUTOSTRUCTURE to minimize the total energies of 2s^{2}2p^6 (2s and 2p orbitals) and 2s^{2}2p^{5}3l (3l orbitals) complexes, respectively – see text for details.

Ion	2s	2p	3s	3p	3d
Na	1.05325	0.99028	1.00144	1.10304	0.89098
Mg	1.06060	0.99638	1.02899	1.07656	0.93850
Al	1.06828	1.00060	1.04887	1.06575	0.96022
Si	1.07620	1.00403	1.06486	1.06016	0.97781
P	1.08461	1.00718	1.07860	1.05719	0.99100
S	1.09407	1.01029	1.09126	1.05619	1.00123
Cl	1.10436	1.01354	1.10346	1.05599	1.00949
Ar	1.11591	1.01700	1.11559	1.05671	1.01639
K	1.12858	1.02117	1.12792	1.05767	1.02320
Ca	1.14291	1.02568	1.14068	1.05846	1.02863
Sc	1.15928	1.03048	1.15407	1.06061	1.03362
Ti	1.17769	1.03588	1.16830	1.06364	1.03784
V	1.19835	1.04209	1.18353	1.06712	1.04196
Cr	1.22166	1.04889	1.19942	1.07165	1.04607
Mn	1.24853	1.05616	1.21647	1.07698	1.05021
Fe	1.27826	1.06471	1.23503	1.08299	1.05443
Co	1.31154	1.07401	1.25541	1.09006	1.05875
Ni	1.35010	1.08401	1.27760	1.09825	1.06316
Cu	1.39467	1.09579	1.30170	1.10729	1.06765
Zn	1.44425	1.10831	1.32832	1.11769	1.07230
Ga	1.50306	1.12207	1.35715	1.12929	1.07705
Ge	1.56998	1.13722	1.38861	1.14226	1.08194
As	1.64873	1.15409	1.42305	1.15656	1.08695
Se	1.74083	1.17262	1.46051	1.17235	1.09212
Br	1.85007	1.19293	1.50166	1.18969	1.09746
Kr	1.98387	1.21520	1.54677	1.20864	1.10295

A comparison of level energies with previous calculations and data, derived semi-empirically from experimental energies, available from the compilation of NIST v3[2] or observed values available in the CHIANTI v6 database and astrophysical modelling code (Dere et al. 2009) was made for several specific ions (Si^{4+}, Ar^{8+}, Ca^{10+}, Fe^{16+}, Ni^{18+} and Kr^{26+}) spanning the sequence so as to assess the accuracy of our present AS calculations over the entire iso-electronic series. Tables 2, 4, 6, 8, 10, and 12 list various theoretical level energies along with NIST

[1] http://www.apap-network.org

[2] http://physics.nist.gov/PhysRefData/ASD/index.html

Table 2. The level energies (Ryd) of Si^{4+} from different calculations along with the compilation of NIST v3[2].

ID	Level specification	NIST[a]	AS	FAC	CHIANTI[b]	MCHF[c]
1	$2s^22p^6\ ^1S_0$		0.000000	0.000000	0.000000	
2	$2s^22p^53s\ ^3P_2$	7.636576	7.627520	7.645096	7.471944	7.636311
3	$2s^22p^53s\ ^3P_1$	7.660020	7.651149	7.669024	7.496347	7.659752
4	$2s^22p^53s\ ^3P_0$	7.682625	7.672594	7.689856	7.518236	7.682296
5	$2s^22p^53s\ ^1P_1$	7.732203	7.727683	7.750462	7.576521	7.731955
6	$2s^22p^53p\ ^3S_1$	8.258379	8.246423	8.256845	8.101019	8.258102
7	$2s^22p^53p\ ^3D_3$	8.364780	8.359913	8.372963	8.189849	8.364501
8	$2s^22p^53p\ ^3D_2$	8.374174	8.369346	8.384104	8.198962	8.373860
9	$2s^22p^53p\ ^3D_1$	8.391529	8.386711	8.399595	8.215911	8.391069
10	$2s^22p^53p\ ^1D_2$	8.422766	8.418290	8.434033	8.250539	8.422583
11	$2s^22p^53p\ ^1P_1$	8.437853	8.436352	8.450207	8.264883	8.437552
12	$2s^22p^53p\ ^3P_2$	8.451074	8.446452	8.462297	8.278670	8.450769
13	$2s^22p^53p\ ^3P_0$	8.454788	8.451684	8.464687	8.280566	8.454470
14	$2s^22p^53p\ ^3P_1$	8.460253	8.457485	8.472367	8.286872	8.459926
15	$2s^22p^53p\ ^1S_0$	8.77505	8.876968	8.922108	8.851711	8.774769
16	$2s^22p^53d\ ^3P_0$	9.273318	9.270566	9.267329	9.103458	9.273033
17	$2s^22p^53d\ ^3P_1$	9.278845	9.276363	9.272374	9.109172	9.278537
18	$2s^22p^53d\ ^3P_2$	9.290708	9.288542	9.284232	9.121027	9.290319
19	$2s^22p^53d\ ^3F_4$	9.307536	9.309413	9.305353	9.132764	9.307223
20	$2s^22p^53d\ ^3F_3$	9.316348	9.318389	9.316576	9.142041	9.316025
21	$2s^22p^53d\ ^3F_2$	9.333562	9.335089	9.332421	9.158398	9.333074
22	$2s^22p^53d\ ^1F_3$	9.345281	9.349206	9.347836	9.172796	9.345075
23	$2s^22p^53d\ ^1D_2$	9.380647	9.383311	9.381456	9.205793	9.379566
24	$2s^22p^53d\ ^3D_1$	9.380036	9.384037	9.383614	9.206276	9.380304
25	$2s^22p^53d\ ^3D_3$	9.384912	9.387550	9.386841	9.210350	9.384568
26	$2s^22p^53d\ ^3D_2$	9.389823	9.392712	9.392014	9.215362	9.389434
27	$2s^22p^53d\ ^1P_1$	9.449065	9.463153	9.471244	9.302779	9.448883
28	$2s^22p^54s\ ^3P_2$	10.01823	10.025722	10.021532		10.017768
29	$2s^22p^54s\ ^3P_1$	10.03067	10.038223	10.036309		10.030362
30	$2s^22p^54s\ ^3P_0$	10.06444	10.070616	10.066578		10.063904
31	$2s^22p^54s\ ^1P_1$	10.07483	10.081318	10.081030		10.074475
32	$2s^22p^54p\ ^3S_1$	10.24486	10.248513	10.246311		
33	$2s^22p^54p\ ^3D_3$	10.27825	10.282198	10.285662		
34	$2s^22p^54p\ ^3D_2$	10.28347	10.287772	10.292513		
35	$2s^22p^54p\ ^1P_1$	10.29257	10.297196	10.302666		
36	$2s^22p^54p\ ^3P_2$	10.29820	10.302854	10.309430		
37	$2s^22p^54p\ ^3P_0$	10.32510	10.330410	10.337097		
38	$2s^22p^54p\ ^3D_1$	10.32766	10.331017	10.335484		
39	$2s^22p^54p\ ^1D_2$	10.33545	10.338814	10.345399		
40	$2s^22p^54p\ ^3P_1$	10.33545	10.339068	10.344921		
41	$2s^22p^54p\ ^1S_0$	10.43362	10.491684	10.528749		
42	$2s^22p^54d\ ^3P_0$	10.59995	10.606728	10.600389		
43	$2s^22p^54d\ ^3P_1$	10.60383	10.610847	10.604652		
44	$2s^22p^54d\ ^3P_2$	10.61133	10.618787	10.613007		
45	$2s^22p^54d\ ^3F_4$	10.61303	10.621538	10.616589		
46	$2s^22p^54d\ ^3F_3$	10.61793	10.626940	10.623125		
47	$2s^22p^54d\ ^1D_2$	10.62689	10.636085	10.632943		
48	$2s^22p^54d\ ^3D_3$	10.63038	10.640347	10.638092		
49	$2s^22p^54d\ ^3D_1$	10.64926	10.661087	10.660041		
50	$2s^22p^54d\ ^3F_2$	10.66570	10.673565	10.670477		
51	$2s^22p^54d\ ^3D_2$	10.66860	10.676813	10.674084		
52	$2s^22p^54d\ ^1F_3$	10.66937	10.677815	10.675137		
53	$2s^22p^54f\ ^3D_1$	10.68445	10.689679	10.689431		
54	$2s^22p^54f\ ^3D_2$	10.68502	10.690324	10.690251		
55	$2s^22p^54f\ ^3G_5$	10.68812	10.694274	10.694413		
56	$2s^22p^54f\ ^1G_4$	10.68821	10.694326	10.694619		
57	$2s^22p^54f\ ^3D_3$	10.69027	10.695958	10.696143		
58	$2s^22p^54f\ ^1D_2$	10.69082	10.696471	10.697012		
59	$2s^22p^54f\ ^1F_3$	10.69390	10.700062	10.700759		
60	$2s^22p^54f\ ^3F_4$	10.69399	10.700209	10.700871		

Notes. [a] Sources of NIST v3 are from the work of Martin & Zalubas (1983) and references therein. [b] Theoretical energies from Bhatia et al. (1985). [c] Data is calculated with multiconfiguration Hartree-Fock (MCHF) or multiconfiguration Dirac-Fock (MCDF) method, and available from website: http://atoms.vuse.vanderbilt.edu/

(v3) derived or CHIANTI (v6) observed ones for the 60 lowest-lying levels. A fully relativistic calculation with the Flexible Atomic Code (FAC, Gu 2008) was also performed for these ions with only CI from $2s^2 2p^4 3l3l'$ included besides that of the CC configurations. This is because a correction of level energies has been carried-out by using the difference of average configuration energy obtained using a different orbital basis for each configuration and that obtained using the unique orbital basis required for multiconfiguration level structure – see Gu (2008) and the FAC manual for details. Such a procedure is not readily usable in an *R*-matrix calculation. A complete comparison with available NIST experimentally derived or CHIANTI observed data is shown in Fig. 1. A complete set of level energies from the present AS calculation is available electronically[3]. Figure 1 and Tables 2, 4, 6, 8, 10, and 12 show that excellent agreement (within 0.5%) is obtained when compared with NIST derived or CHIANTI observed data except for a few energy levels. Moreover, better agreement (0.3%) is obtained for Si^{4+}, Ar^{8+}, Fe^{16+}, Ni^{18+}, etc.

For Si^{4+}, the results of Bhatia et al. (1985) currently used by the CHIANTI are lower than the NIST data by 1.5%–2.3%. The results from multiconfiguration Hartree-Fock (MCHF) or multiconfiguration Dirac-Fock (MCDF) method available from the MCHF/MCDF Collection[4] show excellent agreement with the NIST data. For Ar^{8+}, Ca^{10+} and Ni^{18+}, the calculation of Zhang et al. (1987) was adopted by CHIANTI, showing the same level of accuracy with the present AS calculation. For Fe^{16+}, the present AS data is systematically higher than that of Landi & Gu (2006) used by CHIANTI by ~0.4%. However, both show a better level of accuracy (0.2%) when compared with NIST data. Calculations with the MCDF method have been done for highly charged ions, e.g. Fe^{16+} (Aggarwal et al. 2003), Ni^{18+} (Aggarwal & Keenan 2006) and Kr^{26+} (Griffin et al. 2008) recently. When compared with them, the present AS data agrees also to within 0.4%. This means that our atomic structure is accurate, and the target expansion of 31 spectroscopic configurations and additional 33 correlation configurations in scattering calculation is reliable along the Ne-like iso-electronic sequence.

2.2. Structure: weighted oscillator strength

A further test of our structure calculations is to compare weighted oscillator strengths ($g_i f_{i,j}$ for a given $i \longleftarrow j$ transition, where g_i is statistical weight of the initial level i and f is the oscillator strength of the transition) with those of other calculations. Tables 3, 5, 7, 9, 11, and 13 show a detailed comparison for a selection of gf-values from the 5 lowest-lying levels for six ions spanning the sequence: Si^{4+}, Ar^{8+}, Ca^{10+}, Fe^{16+}, Ni^{18+} and Kr^{26+}.

For Si^{4+}, around 68% of transitions available[5] from the CHIANTI v6 database (Dere et al. 2009) show agreement to within 20% between the present AS calculations and the results of Bhatia et al. (1985). There are about 56% of all-type transitions (this refers to dipole and quadrupole) showing $|1.0 - gf_V/gf_L| \leq 20\%$ with $gf_L \geq 0.001$ (gf_V and gf_L are weighted oscillator strengths in velocity and length gauges, respectively). As shown in Table 3, the present AS calculation also shows good agreement with the results of our FAC calculations and the MCHF ones[4].

Table 3. Comparison of the weighted oscillator strength gf between the AS and other calculations for Si^{4+}.

$i-j$	AS		CHIANTI[a]	FAC	MCHF[b]
	gf_L	gf_V/gf_L			
1–3	2.19^{-2}[c]	0.89	2.36^{-2}	2.09^{-2}	2.44^{-2}
1–5	2.33^{-1}	0.92	2.82^{-1}	2.68^{-1}	2.18^{-1}
1–17	2.63^{-3}	0.94	2.62^{-3}	2.56^{-3}	2.98^{-3}
1–24	7.97^{-2}	0.95	6.54^{-2}	6.23^{-2}	1.03^{-1}
1–27	1.17^{+0}	0.96	1.46^{+0}	1.25^{+0}	1.02^{+0}
2–6	3.58^{-1}	0.86	4.25^{-1}	3.49^{-1}	3.55^{-1}
2–7	1.59^{+0}	0.97	1.54^{+0}	1.58^{+0}	1.55^{+0}
2–8	4.24^{-1}	0.93	4.28^{-1}	4.27^{-1}	4.21^{-1}
2–9	6.08^{-2}	0.89	5.80^{-2}	5.89^{-2}	6.13^{-2}
2–10	5.00^{-1}	0.81	4.89^{-1}	5.20^{-1}	5.16^{-1}
2–11	6.09^{-2}	0.78	5.10^{-2}	5.94^{-2}	4.34^{-2}
2–12	2.91^{-1}	0.75	2.00^{-1}	2.63^{-1}	2.45^{-1}
2–14	1.49^{-1}	0.79	1.27^{-1}	1.55^{-1}	1.55^{-1}
3–6	1.42^{-1}	0.87	1.63^{-1}	1.43^{-1}	1.37^{-1}
3–8	6.92^{-1}	0.99	6.52^{-1}	6.83^{-1}	6.71^{-1}
3–9	4.06^{-1}	0.94	3.92^{-1}	3.91^{-1}	4.05^{-1}
3–10	1.88^{-1}	0.84	2.34^{-1}	2.08^{-1}	2.27^{-1}
3–11	5.58^{-2}	0.79	4.27^{-2}	5.59^{-2}	4.59^{-2}
3–12	2.78^{-1}	0.82	2.18^{-1}	2.61^{-1}	2.30^{-1}
3–13	2.34^{-1}	0.80	2.17^{-1}	2.36^{-1}	2.27^{-1}
3–14	4.86^{-2}	0.72	5.34^{-2}	5.59^{-2}	5.05^{-2}
3–15	2.77^{-2}	0.66	4.09^{-2}	2.42^{-2}	2.60^{-2}
4–6	3.98^{-2}	0.87	4.51^{-2}	3.86^{-2}	3.82^{-2}
4–9	2.13^{-1}	1.02	1.99^{-1}	2.24^{-1}	1.96^{-1}
4–11	2.37^{-1}	0.88	2.27^{-1}	2.07^{-1}	2.13^{-1}
4–14	1.98^{-1}	0.80	1.95^{-1}	2.12^{-1}	2.22^{-1}
5–6	5.06^{-3}	0.81	4.86^{-3}	3.81^{-3}	5.84^{-3}
5–8	1.46^{-2}	1.04	7.84^{-3}	1.39^{-2}	9.49^{-3}
5–9	1.23^{-3}	1.03	1.68^{-3}	7.85^{-4}	1.66^{-3}
5–10	4.89^{-1}	1.02	3.05^{-1}	4.50^{-1}	4.13^{-1}
5–11	3.39^{-1}	0.99	3.11^{-1}	3.65^{-1}	3.73^{-1}
5–12	6.25^{-1}	0.96	7.63^{-1}	6.61^{-1}	6.83^{-1}
5–13	1.39^{-2}	0.84	1.24^{-2}	1.14^{-2}	1.44^{-2}
5–14	3.24^{-1}	0.92	2.83^{-1}	2.96^{-1}	2.79^{-1}
5–15	3.80^{-1}	0.68	5.80^{-1}	3.96^{-1}	3.31^{-1}

Notes. Index number corresponds to that in Table 2.[(a)] Data in CHIANTI are from the work of Bhatia et al. (1985). [(b)] MCHF data is from the website: http://atoms.vuse.vanderbilt.edu/ [(c)] x^y denotes $x \times 10^y$.

For Ar^{8+}, our AS agreement is within 20% when compared with that of Zhang et al. (1987) for 70% of their transitions. The percentage of all-type transition increases up to 78% with $|1.0 - gf_V/gf_L| \leq 20\%$ for this ion. As shown in Table 5, our AS results also show good agreement when compared with the results of FAC and MCHF calculations.

For Ca^{10+}, there are about 76% of transitions with a gf difference within 20% when compared with the data of Zhang et al. (1987). The difference of the present AS gf-values between the velocity and length gauges is also within 20% for 78% of all-type transitions. The comparison with results from the FAC and MCHF methods also shows good agreement, see Table 7.

For Fe^{16+}, there are about 80% of all-type transitions with $|1.0 - gf_V/gf_L| \leq 20\%$. The percentage is 67% of all available transitions from CHIANTI v6 (Dere et al. 2009) with a difference within 20% when compared with those of Landi & Gu (2006). In comparison with results of Aggarwal et al. (2003) from the MCDF method, the percentage is 65%. For the two

[3] http://open.adas.ac.uk/

[4] http://atoms.vuse.vanderbilt.edu/

[5] The percentage refers to the fraction of transitions from the 5 lowest-lying levels to all upper states contained within the cited references.

Table 4. The level energies (Ryd) of Ar^{8+} from different calculations along with the compilation of NIST v3 and CHIANTI v6.

ID	Level specification	NIST/CHIANTI[a]	AS	FAC	CHIANTI[b]	MCHF[c]
1	$2s^22p^6\ ^1S_0$		0.00000			
2	$2s^22p^53s\ ^3P_2$	18.4672	18.4701	18.4879	18.4267	18.4745
3	$2s^22p^53s\ ^3P_1$	18.5271	18.5316	18.5510	18.4823	18.5346
4	$2s^22p^53s\ ^3P_0$	18.6307	18.6318	18.6492	18.5898	18.6377
5	$2s^22p^53s\ ^1P_1$	18.6967	18.7031	18.7249	18.6463	18.7045
6	$2s^22p^53p\ ^3S_1$	19.5859	19.5907	19.6006	19.5898	19.6043
7	$2s^22p^53p\ ^3D_3$	19.7739	19.7862	19.8001	19.7404	19.7945
8	$2s^22p^53p\ ^3D_2$	19.7826	19.7955	19.8113	19.7475	19.8025
9	$2s^22p^53p\ ^3D_1$	19.8049	19.8493	19.8647	19.7960	19.8549
10	$2s^22p^53p\ ^3P_2$	19.8855	19.8968	19.9149	19.8358	19.9050
11	$2s^22p^53p\ ^1P_1$	19.9489	19.9644	19.9775	19.9104	19.9965
12	$2s^22p^53p\ ^3P_0$	19.9751	19.9910	20.0055	19.9271	20.0314
13	$2s^22p^53p\ ^1D_2$	20.0026	20.0131	20.0305	19.9587	19.9685
14	$2s^22p^53p\ ^3P_1$	20.0104	20.0245	20.0413	19.9645	20.0225
15	$2s^22p^53p\ ^1S_0$	20.7851	20.7670	20.8484	20.6289	20.6624
16	$2s^22p^53d\ ^3P_0$	21.4090	21.4282	21.4273	21.3865	21.4359
17	$2s^22p^53d\ ^3P_1$	21.4276	21.4478	21.4451	21.4038	21.4539
18	$2s^22p^53d\ ^3P_2$	21.4650	21.4876	21.4831	21.4403	21.4914
19	$2s^22p^53d\ ^3F_4$	21.4945	21.5229	21.5169	21.4640	21.5230
20	$2s^22p^53d\ ^3F_3$	21.5215	21.5488	21.5475	21.4885	21.5496
21	$2s^22p^53d\ ^3F_2$	21.5794	21.5962	21.5951	21.5314	21.5962
22	$2s^22p^53d\ ^1F_3$	21.6027	21.6352	21.6325	21.5614	21.6305
23	$2s^22p^53d\ ^3D_1$	21.6963	21.7272	21.7266	21.6480	21.7240
24	$2s^22p^53d\ ^1D_2$	21.7091	21.7380	21.7358	21.6690	21.7594
25	$2s^22p^53d\ ^3D_3$	21.7312	21.7616	21.7594	21.6918	21.7622
26	$2s^22p^53d\ ^3D_2$	21.7334	21.7652	21.7632	21.6909	21.7367
27	$2s^22p^53d\ ^1P_1$	21.9709	22.0317	22.0372	21.9433	22.0010
28	$2s2p^63s\ ^3S_1$		24.2031	24.2183	24.1764	24.6381
29	$2s2p^63s\ ^1S_0$		24.4742	24.4911	24.4184	24.7995
30	$2s^22p^54s\ ^3P_2$	24.6131	24.6443	24.6311	24.5969	24.8207
31	$2s^22p^54s\ ^1P_1$	24.6402	24.6718	24.6630	24.6187	24.6671
32	$2s^22p^54s\ ^3P_0$	24.7794	24.8031	24.7905	24.7609	
33	$2s^22p^54s\ ^3P_1$	24.7936	24.8230	24.8145	24.7746	
34	$2s^22p^54p\ ^3S_1$	25.1071	25.1267	25.1214	25.0596	
35	$2s^22p^54p\ ^3D_3$	25.1591	25.1444	25.1408	25.0981	
36	$2s^22p^54p\ ^3D_2$	25.1472	25.1500	25.1479	25.1014	
37	$2s^22p^54p\ ^1P_1$	25.1598	25.1727	25.1722	25.1203	
38	$2s^22p^54p\ ^3P_2$	25.1817	25.1843	25.1849	25.1307	
39	$2s^22p^54p\ ^3P_0$	25.2565	25.2714	25.2739	25.2097	
40	$2s^22p^54p\ ^3D_1$	25.3016	25.3050	25.3021	25.2590	
41	$2s^22p^54p\ ^1D_2$	25.3225	25.3263	25.3258	25.2787	
42	$2s^22p^54p\ ^3P_1$	25.3253	25.3285	25.3284	25.2750	
43	$2s2p^63p\ ^3P_0$		25.5061	25.5425	25.4653	
44	$2s2p^63p\ ^3P_1$	25.3515	25.5140	25.5497	25.4727	
45	$2s2p^63p\ ^3P_2$		25.5355	25.5696	25.4927	
46	$2s^22p^54p\ ^1S_0$	25.5795	25.5741	25.6269	25.4414	
47	$2s2p^63p\ ^1P_1$	25.4298	25.6165	25.6467	25.5656	
48	$2s^22p^54d\ ^3P_0$	25.7158	25.7514	25.7320	25.6922	
49	$2s^22p^54d\ ^3P_1$	25.7260	25.7622	25.7427	25.7023	
50	$2s^22p^54d\ ^3F_4$	25.7417	25.7728	25.7537	25.7187	
51	$2s^22p^54d\ ^3P_2$	25.7448	25.7801	25.7607	25.7205	
52	$2s^22p^54d\ ^3F_3$	25.7552	25.7857	25.7692	25.7305	
53	$2s^22p^54d\ ^1D_2$	25.7753	25.8057	25.7905	25.7478	
54	$2s^22p^54d\ ^3D_3$	25.7859	25.8163	25.8009	25.7560	
55	$2s^22p^54d\ ^3D_1$	25.8443	25.8824	25.8706	25.8135	
56	$2s^22p^54d\ ^3F_2$	25.9173	25.9460	25.9300	25.8927	
57	$2s^22p^54d\ ^3D_2$	25.9255	25.9546	25.9383	25.8973	
58	$2s^22p^54d\ ^1F_3$	25.9312	25.9595	25.9439	25.9037	
59	$2s^22p^54f\ ^3D_1$	25.9443	25.9702	25.9638	25.9250	
60	$2s^22p^54f\ ^3D_2$	25.9487	25.9754	25.9693	25.9276	

Notes. [a] Sources of NIST v3 are from the unpublished work of Shirai et al. (1999), and references therein, while that of CHIANTI v6 is from the work of Lepson et al. (2003). [b] Theoretical energies from Zhang et al. (1987). [c] MCHF data available from the website: `http://atoms.vuse.vanderbilt.edu/`

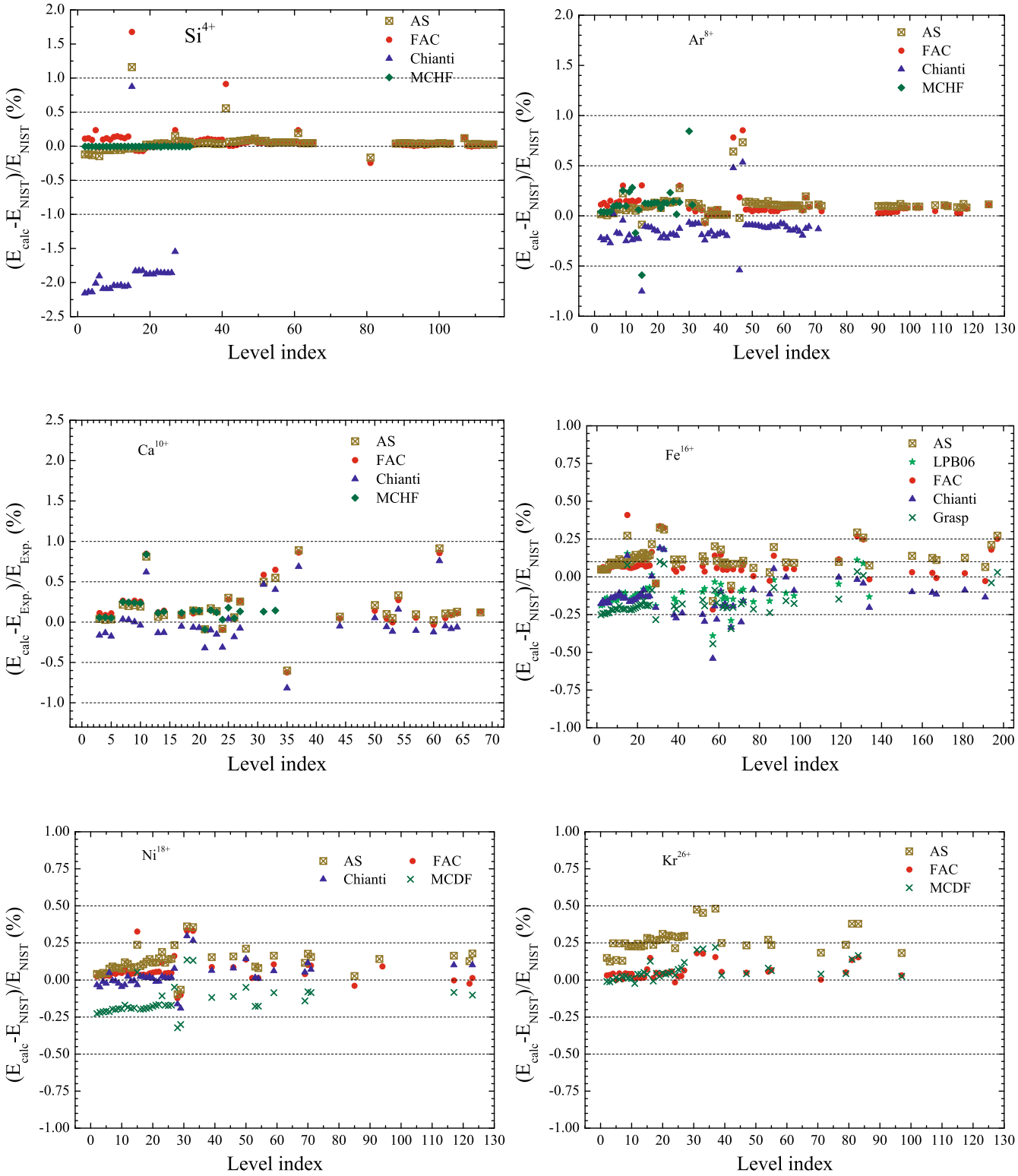

Fig. 1. Comparison of the level energies between the theoretical calculations and the "experimental" data available from NIST or CHIANTI databases. Level index refers to the ID number listed in Tables 2: Si^{4+}; 4: Ar^{8+}; 6: Ca^{10+}; 8: Fe^{16+}; 10: Ni^{18+}, and 12: Kr^{26+}. Labels in each panel corresponds to explanation in Tables of 2,4, 8, 10, and 12, respectively. [*Colour online*]

key transition lines ($3C$ and $3D$), the present AS calculations (2.43 and 5.97×10^{-1}) are slightly lower than the results (2.49 and 6.39×10^{-1}) of Loch et al. 2006) by 2% and 7%, respectively, while those from Chen et al. (2003) obtained from SUPERSTRUCTURE ($3C$–2.57, $3D$–5.90×10^{-1}) and by Landi & Gu (2006) using FAC ($3C$–2.52, $3D$–5.97×10^{-1}) and the present FAC calculation are also within 7%. When pseudo-states were included by Chen (2007) using GRASP2, it results in a slightly larger difference[6] of ~12% ($3C$–2.27, $3D$–6.63×10^{-1}).

For Ni^{18+}, there are about 81% of all-type transitions showing $|1.0 - gf_V/gf_L| \leq 20\%$. When compared with results of

[6] The MCDF level energies of Chen et al. (2003) and the A-values of Chen (2007) are used to derive the gf-values listed here.

Table 5. Comparison of the weighted oscillator strength gf between the AS and other calculations for Ar^{8+}.

$i-j$	AS		CHIANTI[a]	FAC	MCHF[b]
	gf_L	gf_V/gf_L			
1–3	6.75^{-2c}	0.92	1.00^{-1}	6.76^{-2}	6.68^{-2}
1–5	1.79^{-1}	0.96	2.14^{-1}	1.97^{-1}	1.71^{-1}
1–17	4.41^{-3}	0.96	5.90^{-3}	4.73^{-3}	4.96^{-3}
1–23	1.20^{-1}	0.97	1.61^{-1}	1.16^{-1}	1.44^{-1}
1–27	2.06^{+0}	0.97	2.55^{+0}	2.13^{+0}	1.89^{+0}
1–33	2.26^{-2}	0.91	2.72^{-2}	3.14^{-2}	2.31^{-2}
1–47	3.63^{-1}	1.04	2.90^{-1}	4.12^{-1}	
1–55	9.67^{-2}	0.92	1.82^{-1}	8.28^{-2}	
1–67	4.96^{-1}	0.94	5.47^{-1}	5.40^{-1}	
1–181	1.43^{-3}	0.94	2.50^{-3}	1.43^{-3}	
1–183	6.81^{-2}	0.98	1.09^{-1}	7.77^{-2}	
2–6	2.93^{-1}	1.02	2.96^{-1}	2.83^{-1}	2.91^{-1}
2–7	1.13^{+0}	0.97	1.17^{+0}	1.17^{+0}	1.16^{+0}
2–9	6.12^{-2}	0.91	6.67^{-2}	6.69^{-2}	6.56^{-2}
2–14	6.97^{-2}	0.80	8.66^{-2}	8.83^{-2}	8.60^{-2}
2–34	8.29^{-2}	1.23	5.84^{-2}	6.86^{-2}	
2–35	3.48^{-1}	0.98	3.29^{-1}	3.76^{-1}	
2–36	1.02^{-1}	1.00	9.44^{-2}	1.10^{-1}	
2–37	1.51^{-2}	0.98	1.46^{-2}	1.70^{-2}	
2–38	1.32^{-1}	1.06	1.15^{-1}	1.27^{-1}	
2–42	6.92^{-3}	0.91	7.31^{-3}	8.38^{-3}	
3–6	7.04^{-2}	1.06	7.06^{-2}	7.15^{-2}	6.96^{-2}
3–9	3.87^{-1}	0.97	3.92^{-1}	3.80^{-1}	3.88^{-1}
3–10	2.96^{-1}	0.91	3.01^{-1}	3.02^{-1}	3.09^{-1}
3–12	1.52^{-1}	0.85	1.50^{-1}	1.54^{-1}	1.50^{-1}
3–13	7.58^{-2}	0.81	6.33^{-2}	7.65^{-2}	6.30^{-2}
3–14	6.62^{-3}	0.61	7.30^{-3}	8.11^{-3}	7.01^{-3}
3–15	6.97^{-2}	0.71	6.74^{-2}	6.82^{-2}	6.46^{-2}
3–28	2.35^{-1}	0.56	2.40^{-1}	2.41^{-1}	
3–29	4.74^{-2}	0.49	5.12^{-2}	4.39^{-2}	
3–34	4.35^{-3}	1.49	3.69^{-3}	5.02^{-3}	
3–36	1.47^{-1}	0.95	1.37^{-1}	1.53^{-1}	
3–37	1.16^{-1}	0.98	1.10^{-1}	1.20^{-1}	
3–38	7.99^{-2}	1.02	7.53^{-2}	8.33^{-2}	
3–39	3.95^{-2}	1.06	3.62^{-2}	4.02^{-2}	
3–40	3.79^{-3}	1.02	3.18^{-3}	4.19^{-3}	
3–41	2.59^{-2}	1.05	2.31^{-2}	2.89^{-2}	
3–42	2.82^{-3}	1.57	2.17^{-3}	3.29^{-3}	
4–6	1.77^{-2}	1.12	1.77^{-2}	1.76^{-2}	1.75^{-2}
4–9	4.68^{-2}	1.10	3.94^{-2}	5.14^{-2}	4.28^{-2}
4–11	2.48^{-1}	0.95	2.35^{-1}	2.36^{-1}	2.30^{-1}
4–14	1.91^{-1}	0.87	2.12^{-1}	1.96^{-1}	2.08^{-1}
4–28	1.05^{-1}	0.57	1.07^{-1}	1.05^{-1}	
4–37	2.13^{-3}	0.75	1.88^{-3}	2.74^{-3}	
4–40	8.14^{-2}	0.98	7.54^{-2}	8.54^{-2}	
4–42	5.35^{-2}	1.08	4.87^{-2}	5.60^{-2}	
5–6	9.51^{-3}	1.12	1.06^{-2}	8.69^{-3}	1.00^{-2}
5–10	1.04^{-1}	1.10	1.10^{-1}	1.04^{-1}	9.17^{-2}
5–11	2.25^{-1}	1.06	2.42^{-1}	2.32^{-1}	2.41^{-1}
5–12	3.34^{-2}	0.91	3.38^{-2}	3.10^{-2}	3.26^{-2}
5–13	7.29^{-1}	0.97	7.38^{-1}	7.28^{-1}	7.39^{-1}
5–14	2.48^{-1}	0.96	2.25^{-1}	2.40^{-1}	2.27^{-1}
5–36	1.13^{-2}	0.95	1.20^{-2}	1.17^{-2}	
5–37	1.49^{-2}	0.84	1.65^{-2}	1.61^{-2}	
5–38	2.49^{-2}	0.90	2.47^{-2}	2.81^{-2}	
5–39	4.04^{-3}	1.08	4.27^{-3}	4.96^{-3}	
5–40	7.03^{-2}	0.93	6.73^{-2}	7.51^{-2}	
5–42	6.12^{-2}	1.00	5.91^{-2}	6.33^{-2}	
5–46	3.51^{-2}	1.08	3.36^{-2}	3.13^{-2}	

Notes. Index number corresponds to that in Table 4. [(a)] Data in CHIANTI are from the work of Zhang et al. (1987) and Hibbert et al. (1993). [b] MCHF data is from the website: http://atoms.vuse.vanderbilt.edu/ [(c)] x^y denotes $x \times 10^y$.

Aggarwal & Keenan (2006), 68% of electric-dipole transitions show agreement to within 20%. The present AUTOSTRUCTURE calculations show better agreement with those from FAC (83% of transitions) and the data of Zhang et al. (1987), as currently used by CHIANTI v6 (91% of transitions).

For Kr^{26+}, the present results also show good agreement with previous calculations obtained using the MCDF method: Griffin et al. (2008), Rice et al. (2000) and Zhang et al. (1987), see Table 13. The ratio between the present AS gf in length and velocity gauges is within 20% of unity for 72% of all-type transitions. For the $3C$ and $3D$ lines, the present AS results are in close agreement Griffin et al's data (to within 3%).

Thus, we believe that the atomic structure of the ions spanning the sequence is reliable, and expect uncertainty on collision strengths from target structure to be small.

3. Scattering

The scattering calculations were performed using a suite of parallel intermediate-coupling frame transformation *R*-matrix codes (Griffin et al. 1998). Due to the large size of the *R*-matrix "box" (due to the 7d orbital included), we employed 60 basis orbitals to represent the $(N+1)$th-electron continuum per angular momentum for most ions over the sequence. For lower charged ions, the basis orbitals are increased, e.g. 65 for Si^{4+} and P^{5+}, 75 for Al^{3+}, 85 for Mg^{2+} and 95 for Na^{+}. All partial waves from $J = 1/2$ to $81/2$ were included explicitly and contributions from higher J-values were included using a "top-up" procedure (Burgess 1974; Badnell & Griffin 2001). The contributions from partial waves up to $J = 23/2$ were included in the exchange *R*-matrix calculation, while those from $J = 25/2$ to $81/2$ were included via a non-exchange *R*-matrix calculation. For the exchange calculation, a fine energy mesh was used to resolve the dominant resonances below the highest excitation threshold, see Table 14. From just above the highest threshold excitation to a maximum energy of 3.0 times the ionization potential for each ion, a coarse energy mesh ($2.0\times10^{-3}q^2$ Ryd, $q = Z - 10$ is the residual charge of ion) was employed. For the non-exchange calculation, a step of $2.0\times10^{-3}q^2$ Ryd was used over the entire energy range. Witthoeft et al. (2007) tested the convergence of the effective strengths (Υ) with respect to resonance resolutions for several ions spanning the F-like sequence – we adopt the recommended energy meshes of Witthoeft et al. (2007) or better ones, see Table 14.

We then used the infinite energy Born limits (non-dipole allowed) and line-strengths (dipole-allowed) from AUTOSTRUCTURE so that higher energy reduced collision strengths (Ω), as defined by Burgess & Tully (1992), can be found from interpolation in Burgess-Tully space for all additional higher energies. The effective collision strengths at 13 electron temperatures ranging from $2\times10^2(q+1)^2$ K to $2\times10^6(q+1)^2$ K (q is the residual charge of the ion, that is Z-10), are produced as the end product. The data were stored in the ADAS adf04 format (Summers 2004).

4. Results and discussions

4.1. Comparison with previous calculations

We compare the present ICFT *R*-matrix results with those of previous works (DW and/or *R*-matrix) for three ions (Si^{4+}, Fe^{16+} and Kr^{26+}) which span the calculated data for this iso-electronic

Table 6. The level energies (Ryd) of Ca^{10+} from different calculations along with experimental data compiled in CHIANTI v6.

ID	level specification	Exp.[a]	AS	FAC	CHIANTI[b]	MCHF[c]
1	$2s^2 2p6\ ^1S_0$		0.0000	0.0000	0.0000	0.0000
2	$2s^2 2p^5 3s\ ^3P_2$		25.5427	25.5586	25.4991	25.5486
3	$2s^2 2p^5 3s\ ^3P_1$	25.6149	25.6249	25.6435	25.5729	25.6289
4	$2s^2 2p^5 3s\ ^3P_0$	25.8053	25.8126	25.8279	25.7707	25.8205
5	$2s^2 2p^5 3s\ ^1P_1$	25.8791	25.8880	25.9076	25.8335	25.8924
6	$2s^2 2p^5 3p\ ^3S_1$		26.9270	26.9345	26.9288	26.9431
7	$2s^2 2p^5 3p\ ^3D_2$	27.1020	27.1604	27.1738	27.1112	27.1699
8	$2s^2 2p^5 3p\ ^3D_3$	27.1075	27.1613	27.1733	27.1152	27.1738
9	$2s^2 2p^5 3p\ ^1P_1$	27.1813	27.2386	27.2530	27.1819	27.2461
10	$2s^2 2p^5 3p\ ^3P_2$	27.2451	27.2975	27.3143	27.2340	27.3093
11	$2s^2 2p^5 3p\ ^3D_1$	27.2059	27.4268	27.4360	27.3743	27.4337
12	$2s^2 2p^5 3p\ ^3P_0$		27.4440	27.4562	27.3768	27.4516
13	$2s^2 2p^5 3p\ ^1D_2$	27.4893	27.5070	27.5222	27.4526	27.5210
14	$2s^2 2p^5 3p\ ^3P_1$	27.4884	27.5124	27.5273	27.4526	27.5239
15	$2s^2 2p^5 3p\ ^1S_0$		28.3886	28.4770	28.2369	28.2858
16	$2s^2 2p^5 3d\ ^3P_0$		29.1508	29.1489	29.1114	29.1602
17	$2s^2 2p^5 3d\ ^3P_1$	29.1543	29.1812	29.1767	29.1387	29.1880
18	$2s^2 2p^5 3d\ ^3P_2$		29.2418	29.2343	29.1934	29.2443
19	$2s^2 2p^5 3d\ ^3F_4$	29.2344	29.2760	29.2659	29.2152	29.2758
20	$2s^2 2p^5 3d\ ^3F_3$	29.2708	29.3104	29.3071	29.2499	29.3118
21	$2s^2 2p^5 3d\ ^3F_2$	29.4029	29.3772	29.3747	29.3082	29.3764
22	$2s^2 2p^5 3d\ ^3D_3$	29.3765	29.4265	29.4200	29.3474	29.4200
23	$2s^2 2p^5 3d\ ^3D_1$	29.5224	29.5622	29.5594	29.4777	29.5577
24	$2s^2 2p^5 3d\ ^1D_2$	29.6271	29.6026	29.5980	29.5342	29.6361
25	$2s^2 2p^5 3d\ ^3D_2$	29.5506	29.6395	29.6338	29.5624	29.6030
26	$2s^2 2p^5 3d\ ^1F_3$	29.6253	29.6428	29.6366	29.5707	29.6402
27	$2s^2 2p^5 3d\ ^1P_1$	29.9288	30.0051	30.0059	29.9060	29.9684
28	$2s2p^6 3s\ ^3S_1$		32.2654	32.2832	32.2261	
29	$2s2p^6 3s\ ^1S_0$		32.5841	32.6044	32.5190	
30	$2s2p^6 3p\ ^3P_0$		33.8113	33.8432	33.7971	33.6845
31	$2s2p^6 3p\ ^3P_1$	33.6523	33.8206	33.8495	33.8090	33.6960
32	$2s2p^6 3p\ ^3P_2$		33.8508	33.8733	33.8464	33.7327
33	$2s2p^6 3p\ ^1P_1$	33.7981	33.9839	34.0176	33.9338	33.8469
34	$2s^2 2p^5 4s\ ^3P_2$		34.2467	34.2404	34.1543	
35	$2s^2 2p^5 4s\ ^1P_1$	34.4633	34.2563	34.2488	34.1817	
36	$2s^2 2p^5 4s\ ^3P_0$		34.5012	34.4901	34.4277	
37	$2s^2 2p^5 4s\ ^3P_1$	34.2082	34.5124	34.5026	34.4432	
38	$2s^2 2p^5 4p\ ^3S_1$		34.7857	34.7746	34.7320	
39	$2s^2 2p^5 4p\ ^3D_3$		34.8251	34.8174	34.7818	
40	$2s^2 2p^5 4p\ ^3D_2$		34.8270	34.8207	34.7802	
41	$2s^2 2p^5 4p\ ^1P_1$		34.8601	34.8562	34.8074	
42	$2s^2 2p^5 4p\ ^3P_2$		34.8770	34.8745	34.8230	
43	$2s^2 2p^5 4p\ ^3P_0$		35.0069	35.0089	34.9386	
44	$2s^2 2p^5 4p\ ^3D_1$	35.0628	35.0862	35.0788	35.0446	
45	$2s^2 2p^5 4p\ ^1D_2$		35.1190	35.1149	35.0754	
46	$2s^2 2p^5 4p\ ^3P_1$		35.1201	35.1165	35.0691	
47	$2s^2 2p^5 4p\ ^1S_0$		35.3734	35.4243	35.2506	
48	$2s^2 2p^5 4d\ ^3P_0$		35.5595	35.5355	35.5085	
49	$2s^2 2p^5 4d\ ^3P_1$		35.5757	35.5516	35.5230	
50	$2s^2 2p^5 4d\ ^3F_4$	35.5245	35.5992	35.5751	35.5431	
51	$2s^2 2p^5 4d\ ^3P_2$		35.6032	35.5793	35.5477	
52	$2s^2 2p^5 4d\ ^3F_3$	35.5799	35.6149	35.5945	35.5586	
53	$2s^2 2p^5 4d\ ^1D_2$	35.6233	35.6407	35.6217	35.5814	
54	$2s^2 2p^5 4d\ ^3D_3$	35.5377	35.6551	35.6352	35.5932	
55	$2s^2 2p^5 4f\ ^3D_1$		35.7173	35.7076	35.8297	
56	$2s^2 2p^5 4f\ ^3D_2$		36.1749	35.7228	35.8340	
57	$2s^2 2p^5 4d\ ^3D_1$	35.7126	35.7469	35.7315	35.6752	
58	$2^s 2p^6 3d\ ^3D_3$		35.7674	35.7553	35.9009	
59	$2s^2 2p^5 4f\ ^1D_2$		35.7339	35.8565	35.8347	
60	$2s^2 2p^5 4d\ ^3F_2$	35.8730	35.8811	35.8612	35.8283	

Notes. [a] E xperimental data are from the CHIANTI v6 database – see references therein. [b] Theoretical energies from Zhang et al. (1987). [c] MCHF data is available from the website: http://atoms.vuse.vanderbilt.edu/

sequence. Here, we select the extensively studied transition line $3D$ as a sensitive test of the accuracy of the present ICFT *R*-matrix calculation, and give special attention to the cosmic abundant ion–Fe^{16+}. (The $3C$ line is less sensitive to the collision method because its excitation is more strongly non-resonant, but we show a comparison with experiment for Fe^{16+} along with $3D$.) An extensive comparison (all available excitation data from ground state $2s^22p^6\ ^1S_0$) between the present ICFT *R*-matrix and previous calculations (with preference to data with resonances included) has been made for the three ions to test widespread of accuracy of the present ICFT *R*-matrix data.

— Si^{4+} To our best knowledge, there is no *R*-matrix data available. The DW data of (Bhatia et al. 1985, with only ground and $2s^22p^53l$ configurations included) was extensively used by current modelling codes, including CHIANTI v6. For the $3D$ line as shown in Fig. 2, the data from the DW calculations (Bhatia et al. (1985) at E_e = 204.09 eV, and the present FAC calculation) agrees with the background cross-section (σ) of the present ICFT *R*-matrix calculation to within 20%. Below the electron energy of E_e = 150 eV, the data of FAC is slightly higher than the background of the present ICFT *R*-matrix calculation. At low temperatures $T_e < 1.0 \times 10^5$ K, the present ICFT Υ is higher than that of Bhatia et al. (1985) by ~80%, however, it is in agreement with the FAC calculation. At the temperature ($T_e = 1.6 \times 10^5$ K) with peak abundance in ionization equilibrium (Mazzotta et al. 1998; Bryans et al. 2006); Bhatia et al.'s data is lower than the present ICFT data by ~40%. The FAC result shows an excellent agreement with the present ICFT result. Above the temperature of $T_e = 1.0 \times 10^6$ K, the difference between the present Υ and the result of Bhatia et al. (1985) is about ~45%. This is higher than the general assessment criteria for the $3D$ transition as in cases of Fe^{16+} and Kr^{26+} discussed at following. This discrepancy at high temperatures is due to lower cross-sections from the DW calculation at high energies where the line strength (S) dominates the cross-section. This is consistent with the difference of the collision strength limit–$4gf/E_{ij} = 4S/3$ for this transition (AS: 3.39×10^{-2}; FAC: 2.65×10^{-2}; Bhatia et al. 1985: 2.84×10^{-2}, MCHF[4]: 4.39×10^{-2}, see Table 3). The present AS calculation is within the range of the low (FAC) and high (MCHF) cases. Moreover, the excellent agreement of level energies between the present AUTOSTRUCTURE calculation and NIST data give more confidence to the present ICFT *R*-matrix calculation.

An extensive comparison with the results of Bhatia et al. (1985) is made in Fig. 3. At a low temperature of $T_e = 2.5 \times 10^4$ K, all available excitation data (DW) of Bhatia et al. (1985) from the ground state is lower than the present ICFT *R*-matrix calculation, and only 4% of them are within 20%. At the temperature (1.6×10^5 K) of peak fractional abundance in ionization equilibrium (Mazzotta et al. 1998; Bryans et al. 2006), the percentage increases to 19%. At a high temperature of $T_e = 2.5 \times 10^6$ K, 50% of excitations from the ground state show agreement to within 20%.

— Fe^{16+} Many calculations have been done with resonances taken into account, such as the serial work of Chen et al. (2003, 2006), Chen (2007), Aggarwal et al. (2003), Loch et al. (2006), and Landi & Gu (2006). In Fig. 4, we present the comparison of cross-sections and effective collision strengths Υ with previous available data, for the $3D$-excitation (1–23). In the work of Loch et al. (2006), a finer energy mesh of about 10 times present case was employed to test the convergence of the Υ relative to the resolution of resonances. They concluded that the effect is quite small when compared with their results obtained with a coarser energy mesh (20 000 points in the

Table 7. Comparison of the weighted oscillator strength gf between the AS and other calculations for Ca^{10+}.

$i-j$	AS		CHIANTI[a]	FAC	MCHF[b]
	gf_L	gf_V/gf_L			
1–3	9.05^{-2}	0.93	1.09^{-1}	9.16^{-2}	8.77^{-2}
1–5	1.50^{-1}	0.96	1.60^{-1}	1.64^{-1}	1.46^{-1}
1–17	5.74^{-3}	0.97	7.20^{-3}	6.29^{-3}	6.44^{-3}
1–23	1.86^{-1}	0.98	2.34^{-1}	1.85^{-1}	2.17^{-1}
1–27	2.29^{+0}	0.98	2.68^{+0}	2.35^{+0}	2.12^{+0}
1–31	1.00^{-2}	0.98	1.07^{-2}	1.04^{-2}	9.10^{-3}
1–33	2.94^{-1}	1.05	3.10^{-1}	3.11^{-1}	2.70^{-1}
1–35	1.04^{-2}	0.76	3.09^{-2}	1.23^{-2}	
1–37	8.93^{-3}	0.87	2.26^{-2}	1.22^{-2}	
1–49	3.25^{-3}	0.94	3.70^{-3}	3.65^{-3}	
1–181	2.13^{-3}	0.96	5.10^{-3}	2.39^{-3}	
1–183	6.46^{-2}	0.99	1.14^{-1}	7.17^{-2}	
2–6	2.72^{-1}	1.07	2.78^{-1}	2.68^{-1}	2.75^{-1}
2–7	3.16^{-1}	0.97	3.15^{-1}	3.21^{-1}	3.18^{-1}
2–8	1.04^{+0}	0.97	1.04^{+0}	1.04^{+0}	1.03^{+0}
2–9	5.83^{-2}	0.93	5.62^{-2}	5.86^{-2}	5.61^{-2}
2–13	2.90^{-2}	0.75	3.03^{-2}	2.89^{-2}	2.66^{-2}
2–14	6.45^{-2}	0.80	6.40^{-2}	6.54^{-2}	6.25^{-2}
2–38	1.38^{-1}	1.04	4.71^{-1}	1.43^{-1}	
2–39	4.24^{-1}	0.98	3.93^{-1}	4.43^{-1}	
2–41	1.53^{-2}	1.00	1.46^{-2}	1.68^{-2}	
2–42	1.55^{-1}	1.04	1.44^{-1}	1.57^{-1}	
2–46	4.06^{-3}	1.07	3.79^{-3}	4.56^{-3}	
3–6	4.84^{-2}	1.12	4.89^{-2}	4.92^{-2}	4.79^{-2}
3–7	4.06^{-1}	1.04	4.07^{-1}	3.99^{-1}	3.99^{-1}
3–9	3.70^{-1}	1.00	3.71^{-1}	3.67^{-1}	4.01^{-1}
3–11	6.55^{-3}	1.01	4.90^{-3}	6.92^{-3}	5.33^{-3}
3–12	1.26^{-1}	0.86	1.26^{-1}	1.27^{-1}	1.26^{-1}
3–13	3.51^{-2}	0.79	2.91^{-2}	3.66^{-2}	2.98^{-2}
3–14	1.27^{-3}	0.44	1.90^{-3}	1.76^{-3}	1.52^{-3}
3–15	8.37^{-2}	0.72	7.95^{-2}	8.36^{-2}	7.66^{-2}
3–28	1.71^{-1}	0.52	1.77^{-1}	1.75^{-1}	
3–29	6.18^{-2}	0.47	6.58^{-2}	5.85^{-2}	
3–38	1.38^{-2}	1.03	1.33^{-2}	1.56^{-2}	
3–41	1.54^{-1}	0.97	1.46^{-1}	1.59^{-1}	
3–42	1.07^{-1}	1.01	1.01^{-1}	1.11^{-1}	
3–43	4.56^{-2}	1.05	4.21^{-2}	4.59^{-2}	
3–44	2.42^{-3}	1.03	2.04^{-3}	2.67^{-3}	
3–46	2.33^{-3}	1.33	1.96^{-3}	2.71^{-3}	
4–6	1.12^{-2}	1.25	1.13^{-2}	1.12^{-2}	1.11^{-2}
4–11	2.20^{-1}	0.98	2.05^{-1}	2.13^{-1}	2.05^{-1}
4–14	1.97^{-1}	0.90	2.14^{-1}	2.01^{-1}	2.11^{-1}
4–28	8.84^{-2}	0.55	9.12^{-2}	8.79^{-2}	
4–38	1.35^{-3}	0.99	1.18^{-3}	1.69^{-3}	
4–41	1.20^{-3}	0.75	1.09^{-3}	1.54^{-3}	
4–44	9.03^{-2}	0.97	8.44^{-2}	9.45^{-2}	
4–46	7.91^{-2}	1.03	7.27^{-2}	8.16^{-2}	
4–55	2.18^{-3}	0.93	2.18^{-3}	2.41^{-3}	
5–6	9.03^{-3}	1.26	9.60^{-3}	8.52^{-3}	9.20^{-3}
5–11	2.06^{-1}	1.08	2.20^{-1}	2.09^{-1}	2.18^{-1}
5–12	3.89^{-2}	0.94	3.80^{-2}	3.71^{-2}	3.71^{-2}
5–13	7.01^{-1}	0.98	7.04^{-1}	6.99^{-1}	7.03^{-1}
5–14	2.10^{-1}	0.98	1.92^{-1}	2.05^{-1}	1.94^{-1}
5–15	1.96^{-1}	0.75	1.87^{-1}	2.06^{-1}	1.86^{-1}
5–28	9.73^{-2}	0.56	9.89^{-2}	9.26^{-2}	
5–29	1.01^{-1}	0.52	1.10^{-1}	9.97^{-2}	
5–41	8.93^{-3}	0.83	1.02^{-2}	9.82^{-3}	
5–44	9.30^{-2}	0.94	8.84^{-2}	9.78^{-2}	
5–45	2.80^{-1}	0.98	2.64^{-1}	2.89^{-1}	
5–46	7.79^{-2}	0.99	7.52^{-2}	8.07^{-2}	
5–47	3.92^{-2}	1.10	3.63^{-2}	3.62^{-2}	

Notes. Index number corresponds to that in Table 6. [(a)] Data in CHIANTI from the work of Zhang et al. (1987) and Hibbert et al. (1993). [(b)] Data is calculated with multiconfiguration Hartree-Fock (MCHF) or multiconfiguration Dirac-Fock (MCDF) method, and available from the website: http://atoms.vuse.vanderbilt.edu/ [(c)] x^y denotes $x \times 10^y$.

Table 8. The level energies (Ryd) of Fe^{16+} from different calculations along with the compilation of NIST v3.

ID	Level specification	NIST[a]	AS	FAC	MCDF[b]	CHIANTI[c]	LPB06[d]
1	$2s^22p^6\ ^1S_0$						
2	$2s^22p^5 3s\ ^3P_2$	53.3045	53.3307	53.3312	53.1706	53.2094	53.2031
3	$2s^22p^5 3s\ ^1P_1$	53.4437	53.4689	53.4779	53.3143	53.3568	53.3448
4	$2s^22p^5 3s\ ^3P_0$	54.2314	54.2578	54.2560	54.0986	54.1357	54.1517
5	$2s^22p^5 3s\ ^3P_1$	54.3194	54.3462	54.3496	54.1897	54.2300	54.2431
6	$2s^22p^5 3p\ ^3S_1$	55.5276	55.5708	55.5563	55.3951	55.4308	55.4328
7	$2s^22p^5 3p\ ^3D_2$	55.7849	55.8376	55.8272	55.6636	55.7067	55.6964
8	$2s^22p^5 3p\ ^3D_3$	55.9038	55.9520	55.9426	55.7804	55.8246	55.8201
9	$2s^22p^5 3p\ ^1P_1$	55.9869	56.0364	56.0320	55.8682	55.9135	55.9022
10	$2s^22p^5 3p\ ^3P_2$	56.1201	56.1639	56.1619	55.9989	56.0474	56.0335
11	$2s^22p^5 3p\ ^3P_0$	56.5191	56.5849	56.5719	56.4098	56.4579	56.4508
12	$2s^22p^5 3p\ ^3D_1$	56.6718	56.7311	56.7111	56.5526	56.6006	56.6084
13	$2s^22p^5 3p\ ^3P_1$	56.9105	56.9573	56.9494	56.7885	56.8289	56.8445
14	$2s^22p^5 3p\ ^1D_2$	56.9383	56.9872	56.9778	56.8171	56.8582	56.8772
15	$2s^22p^5 3p\ ^1S_0$	57.8965	58.0542	58.1335	57.9419	57.9776	57.9856
16	$2s^22p^5 3d\ ^3P_0$	58.9041	58.9616	58.9393	58.7755	58.8068	58.8127
17	$2s^22p^5 3d\ ^3P_1$	58.9754	59.0393	59.0102	58.8470	58.8790	58.8896
18	$2s^22p^5 3d\ ^3P_2$	59.1084	59.1836	59.1458	58.9838	59.0170	59.0303
19	$2s^22p^5 3d\ ^3F_4$	59.1123	59.1979	59.1518	58.9913	59.0242	59.0417
20	$2s^22p^5 3d\ ^3F_3$	59.1688	59.2402	59.2122	59.0521	59.0874	59.0991
21	$2s^22p^5 3d\ ^1D_2$	59.2934	59.3676	59.3423	59.1821	59.2187	59.2247
22	$2s^22p^5 3d\ ^3D_3$	59.3722	59.4603	59.4210	59.2625	59.3014	59.3077
23	$2s^22p^5 3d\ ^3D_1$	59.7080	59.8023	59.7720	59.6131	59.6558	59.6588
24	$2s^22p^5 3d\ ^3F_2$	60.0922	60.1639	60.1337	59.9778	60.0127	60.0446
25	$2s^22p^5 3d\ ^3D_2$	60.1523	60.2362	60.1962	60.0370	60.0718	60.1031
26	$2s^22p^5 3d\ ^1F_3$	60.1906	60.2777	60.2357	60.0784	60.1136	60.1476
27	$2s^22p^5 3d\ ^1P_1$	60.6904	60.8214	60.7903	60.6368	60.6927	60.6979
28	$2s2p^6 3s\ ^3S_1$		63.3645	63.3648	63.2124	63.2696	63.2710
29	$2s2p^6 3s\ ^1S_0$	63.8798	63.8515	63.8514	63.6988	63.7498	63.7572
30	$2s2p^6 3p\ ^3P_0$		65.7796	65.7877	65.6342	65.6924	65.6910
31	$2s2p^6 3p\ ^3P_1$	65.6012	65.8153	65.8214	65.6674	65.7260	65.7266
32	$2s2p^6 3p\ ^3P_2$		65.9876	65.9901	65.8373	65.8944	65.9017
33	$2s2p^6 3p\ ^1P_1$	65.9238	66.1298	66.1379	65.9800	66.0421	66.0427
34	$2s2p^6 3d\ ^3D_1$		69.0895	69.0653	68.9199	68.9602	68.9884
35	$2s2p^6 3d\ ^3D_2$		69.1085	69.0752	68.9299	68.9704	69.0021
36	$2s2p^6 3d\ ^3D_3$		69.1411	69.0942	68.9492	68.9891	69.0244
37	$2s2p^6 3d\ ^1D_2$		69.4869	69.4588	69.3246	69.3763	69.3962
38	$2s^22p^5 4s\ ^3P_2$	71.7987	71.8811	71.8355	71.6597	71.6171	71.6967
39	$2s^22p^5 4s\ ^1P_1$	71.8607	71.9220	71.8848	71.7069	71.6641	71.7432
40	$2s^22p^5 4p\ ^3S_1$		72.7994	72.7615	72.5911	72.5318	72.6254
41	$2s^22p^5 4s\ ^3P_0$		72.8081	72.7629	72.5874	72.5469	72.6500
42	$2s^22p^5 4s\ ^3P_1$	72.7464	72.8295	72.7883	72.6153	72.5710	72.6746
43	$2s^22p^5 4p\ ^3D_2$		72.8634	72.8319	72.6530	72.6004	72.6897
44	$2s^22p^5 4p\ ^3D_3$		72.9087	72.8792	72.7022	72.6435	72.7416
45	$2s^22p^5 4p\ ^1P_1$		72.9373	72.9115	72.7323	72.6753	72.7699
46	$2s^22p^5 4p\ ^3P_2$		72.9786	72.9557	72.7756	72.7170	72.8132
47	$2s^22p^5 4p\ ^3P_0$		73.2551	73.2511	73.0634	72.9940	73.1028
48	$2s^22p^5 4p\ ^3D_1$		73.7730	73.7383	73.5649	73.5003	73.6243
49	$2s^22p^5 4p\ ^3P_1$		73.8526	73.8255	73.6515	73.5963	73.7118
50	$2s^22p^5 4p\ ^1D_2$		73.8697	73.8431	73.6682	73.6135	73.7296
51	$2s^22p^5 4d\ ^3P_0$		74.0252	73.9790	73.8125	73.7417	73.8512
52	$2s^22p^5 4d\ ^3P_1$	73.9584	74.0590	74.0119	73.8449	73.7727	73.8853
53	$2s^22p^5 4d\ ^3F_4$	74.0277	74.1043	74.1091	73.8853	73.8308	73.9701
54	$2s^22p^5 4p\ ^1S_0$		74.0833	74.0531	73.9148	73.8083	73.9491
55	$2s^22p^5 4d\ ^3P_2$		74.1140	74.0660	73.8982	73.8224	73.9396
56	$2s^22p^5 4d\ ^3F_3$		74.1195	74.0767	73.9075	73.8364	73.9283
57	$2s^22p^5 4d\ ^1D_2$	74.2838	74.1644	74.1236	73.9538	73.8813	73.9939
58	$2s^22p^5 4d\ ^3D_3$	74.0477	74.1970	74.1519	73.9819	73.9044	74.0231
59	$2s^22p^5 4d\ ^3D_1$	74.3047	74.3832	74.3478	74.1765	74.0944	74.2181
60	$2s^22p^5 4f\ ^3D_1$		74.6746	74.6503	74.4623	74.4692	74.5017

Notes. [a] Sources of the NIST v3 are from the work of Sugar & Corliss (1985) and references therein. [b] MCDF data from the work of Aggarwal et al. (2004). [c] Data in CHIANTI are from the work of Landi & Gu (2006). [d] LPB06 corresponds to the work of Loch et al. (2006).

Table 9. Comparison of the weighted oscillator strength gf between the AS and other calculations for Fe^{16+}.

$i-j$	AS		GRASP[a]	CHIANTI[b]	FAC	SS[c]
	gf_L	gf_V/gf_L				
1–3	1.25^{-1}	0.91	1.26^{-1}	1.23^{-1}	1.27^{-1}	1.24^{-1}
1–5	1.02^{-1}	0.97	1.07^{-1}	1.06^{-1}	1.10^{-1}	1.02^{-1}
1–17	8.77^{-3}	0.97	9.94^{-3}	9.96^{-3}	1.01^{-2}	8.70^{-3}
1–23	5.97^{-1}	0.99	6.18^{-1}	5.97^{-1}	6.09^{-1}	5.90^{-1}
1–27	2.43^{+0}	0.99	2.56^{-0}	2.52^{+0}	2.46^{+0}	2.57^{+0}
1–31	3.54^{-2}	1.01	3.55^{-2}	3.37^{-2}	3.57^{-2}	3.15^{-2}
1–42	1.42^{-2}	0.92	1.84^{-2}	1.64^{-2}	1.83^{-2}	1.49^{-2}
1–52	3.41^{-3}	0.95	3.94^{-3}	4.53^{-3}	4.03^{-3}	3.57^{-3}
1–59	3.70^{-1}	0.96	4.13^{-1}	3.76^{-1}	3.82^{-1}	4.08^{-1}
1–71	4.24^{-1}	0.97	5.10^{-1}	4.36^{-1}	4.60^{-1}	4.95^{-1}
1–129	1.25^{-2}	0.93	1.69^{-2}	1.21^{-2}	1.37^{-2}	
1–131	9.39^{-2}	0.97	1.11^{-1}	8.98^{-2}	1.03^{-1}	
2–6	2.51^{-1}	1.20	2.55^{-1}	2.52^{-1}	2.48^{-1}	2.52^{-1}
2–7	2.53^{-1}	1.05	2.60^{-1}	2.57^{-1}	2.54^{-1}	2.60^{-1}
2–8	8.07^{-1}	0.99	8.23^{-1}	8.06^{-1}	8.02^{-1}	8.12^{-1}
2–9	1.89^{-2}	0.98	1.92^{-2}	1.93^{-2}	1.91^{-2}	
2–40	2.36^{-1}	0.97	2.34^{-1}	2.35^{-1}	2.45^{-1}	
2–43	1.88^{-1}	0.97	1.90^{-1}	1.91^{-1}	2.00^{-1}	
2–44	5.69^{-1}	0.97	5.55^{-1}	5.62^{-1}	5.87^{-1}	
2–46	2.00^{-1}	1.01	1.92^{-1}	1.94^{-1}	2.00^{-1}	
3–6	1.10^{-2}	1.24	1.10^{-2}	1.11^{-2}	1.11^{-2}	
3–7	2.84^{-1}	1.13	2.85^{-1}	2.79^{-1}	2.78^{-1}	2.84^{-1}
3–9	3.19^{-1}	1.07	3.25^{-1}	3.19^{-1}	3.17^{-1}	3.22^{-1}
3–10	2.73^{-1}	0.96	2.83^{-1}	2.77^{-1}	2.75^{-1}	2.81^{-1}
3–11	9.96^{-2}	0.89	1.02^{-1}	1.03^{-1}	9.94^{-2}	1.02^{-1}
3–12	1.53^{-3}	1.21	1.38^{-3}	1.36^{-3}	1.32^{-3}	
3–14	4.15^{-3}	0.61	4.53^{-3}	4.61^{-3}	4.76^{-3}	
3–15	7.84^{-2}	0.72	8.05^{-2}	7.06^{-2}	8.00^{-2}	7.93^{-2}
3–28	9.23^{-2}	0.44	9.74^{-2}	1.01^{-1}	9.51^{-2}	
3–29	7.35^{-2}	0.34	7.72^{-2}	7.87^{-2}	7.17^{-2}	
3–43	2.33^{-1}	0.94	2.29^{-1}	2.29^{-1}	2.38^{-1}	
4–6	2.20^{-3}	1.62	2.23^{-3}	2.23^{-3}	2.20^{-3}	
4–12	1.30^{-1}	0.94	1.31^{-1}	1.32^{-1}	1.28^{-1}	
4–13	2.07^{-1}	0.83	2.12^{-1}	2.10^{-1}	2.07^{-1}	
4–28	6.41^{-2}	0.51	6.59^{-2}	6.76^{-2}	6.39^{-2}	
4–48	8.96^{-2}	0.96	8.88^{-2}	8.86^{-2}	9.33^{-2}	
4–49	1.49^{-1}	1.03	1.46^{-1}	1.48^{-1}	1.54^{-1}	
5–6	6.25^{-3}	2.17	2.83^{-3}	2.87^{-3}	2.78^{-3}	
5–10	6.54^{-3}	1.48	4.67^{-3}	4.73^{-3}	4.76^{-3}	
5–11	3.39^{-2}	1.11	3.10^{-2}	2.98^{-2}	3.00^{-2}	
5–12	2.14^{-1}	1.15	1.89^{-1}	1.87^{-1}	1.83^{-1}	
5–14	5.82^{-1}	1.00	5.93^{-1}	5.85^{-1}	5.78^{-1}	5.89^{-1}
5–15	1.05^{-1}	0.82	1.34^{-1}	1.19^{-1}	1.33^{-1}	1.33^{-1}
5–28	5.47^{-2}	0.53	1.05^{-1}	1.07^{-1}	1.01^{-1}	
5–29	2.33^{-2}	0.42	5.73^{-2}	5.96^{-2}	5.38^{-2}	
5–47	3.64^{-3}	0.91	5.11^{-3}	4.45^{-3}	5.75^{-3}	
5–49	7.80^{-2}	0.98	7.92^{-2}	7.76^{-2}	8.18^{-2}	

Notes. Index number corresponds to that in Table 8.[(a)] GRASP data from the work of Aggarwal et al. (2004). [(b)] Data in CHIANTI are from the work of Landi & Gu (2006). [(c)] The SUPERSTRUCTURE (SS) calculations are from the work of Chen et al. (2003). [(d)] x^y denotes $x \times 10^y$.

resonance region, comparable to our present ICFT *R*-matrix calculation). Good agreement is obtained between the present results and those of Loch et al. for the background cross-section (e.g. ~10% at an electron energy of 1100 eV). The cross-section convoluted by a Gaussian profile (a width of 30 eV, comparable with resolution of present detectors in the laboratory) also shows agreement except for that around energies of 870 eV. At energies of 910 eV and 964 eV, the present ICFT *R*-matrix results show a better agreement (6% and 19%) with laboratory measurement (Brown et al. 2006) than results of Chen (2007, 24% and 28%) and Loch et al. (2006, 26% and 33%). This results in a slightly lower Υ than previous results, see Fig. 4-b. An isolated resonance approximation has been employed by Landi & Gu (2006) to take the resonances in electron-impact excitation into account. However, their Υ at lower temperatures ($T_e \leq 2 \times 10^6$ K) is far above that from the present calculation, by up to 30% around $T_e = 2.9 \times 10^5$ K. At higher temperatures, their results show good agreement with Chen's and Loch et al.'s data, as well as the present ICFT *R*-matrix calculations (to within 10%). Landi & Gu (2006) data is currently used by the astrophysical modelling code-CHIANTI v6. Over the entire temperature range, the Dirac *R*-matrix calculation of Loch et al. (2006) is slightly higher than the present ICFT *R*-matrix calculation, by about 7%, which is consistent with the difference level of atomic structure, e.g. the gf-value discussed above in Sect. 2.2.

For the stronger $3C$ excitation (1–27), see Fig. 5, the present ICFT *R*-matrix results agree well (better than 5%) with those from the DARC calculation performed by Loch et al. (2006) at the energies of 910 and 964 eV. Both are higher than the measurement (Brown et al. 2006) by ~35%. For the DARC calculation of Chen (2007), the difference drops to about 20% when compared with experimental data. This mirrors the reduction in his reported A-values, and the weighted oscillator strengths shown above, due to the inclusion of target pseudo-states – a similar effect was noted by Fournier & Hansen (2005). The present result is also in agreement (8%) with that reported by Aggarwal et al. (2003), see the point at $E_e = 1020$ eV. The resulting effective collision strengths also show good agreement (about 7%) between the present results and the BPRM of Chen et al. (2003) and DARC of Loch et al. (2006) over temperatures of equilibrium abundance for Fe^{16+}. With decreasing electron temperature, the difference between the present results and the DW plus isolated resonance results of Landi & Gu (2006) increases, but is still less than 20% at $T_e = 2.9 \times 10^5$ K. The DARC results of Chen (2007) are slightly lower than the present ones, by about 10%.

A complete set of data for Fe^{16+} for the work of Loch et al. (2006) is available from the Oak Ridge National Laboratory (ORNL) Controlled Fusion Atomic Data Center (CFADC)[7] and for Landi & Gu (2006) from CHIANTI v6. Thus, we make an extensive comparison (all excitation data from ground state $2s^2 2p^6\ ^1S_0$) with them at low (3.0×10^5 K), intermediate (4.0×10^6 K) and high (1.0×10^7 K) temperatures, see Fig. 6. In this comparison, we take configuration, total angular momentum J and energy ordering as the "good" quantum numbers, following the work of Liang et al. (2009b) for the Na-like iso-electronic sequence. At the low temperature, 61% and 92% of transitions (circles in top panel of Fig. 6) show agreement of 20% and a factor of 2, respectively. And there is a trend that more weaker excitations show larger differences. However, the comparison with results from the isolated resonant approximation reveals that only 25% and 64% of transitions show agreement of 20% and a factor of 2, respectively. Most excitation data (87%) of Landi & Gu (2006) is lower than the present ICFT *R*-matrix calculations. As explained in our assessment of atomic structure, the difference in structure can not explain this large discrepancy. This suggests that the systematic lower values for Υ may be

[7] http://www-cfadc.phy.ornl.gov/

Table 10. The level energies (Ryd) of Ni^{18+} from different calculations along with the compilation of NIST v3.

ID	Level specification	NIST[a]	AS	FAC	GRASP[b]	CHIANTI[c]
1	$2s^22p^6\ ^1S_0$		0.00000		0.0000	
2	$2s^22p^53s\ ^3P_2$	64.7479	64.7742	64.6221	64.6011	64.7263
3	$2s^22p^53s\ ^1P_1$	64.9059	64.9287	64.7897	64.7640	64.8740
4	$2s^22p^53s\ ^3P_0$	66.0459	66.0775	65.9187	65.9039	66.0385
5	$2s^22p^53s\ ^3P_1$	66.1407	66.1706	66.0193	66.0009	66.1251
6	$2s^22p^53p\ ^3S_1$	67.2696	67.3214	67.1650	67.1257	67.3018
7	$2s^22p^53p\ ^3D_2$	67.5241	67.5856	67.4291	67.3913	67.5202
8	$2s^22p^53p\ ^3D_3$	67.7229	67.7786	67.6269	67.5876	67.7173
9	$2s^22p^53p\ ^1P_1$	67.7987	67.8544	67.7073	67.6682	67.7830
10	$2s^22p^53p\ ^3P_2$	67.9647	68.0153	67.8694	67.8324	67.9334
11	$2s^22p^53p\ ^3P_0$	68.4879	68.5694	68.4048	68.3717	68.4646
12	$2s^22p^53p\ ^3D_1$	68.7711	68.8455	68.6775	68.6441	68.7870
13	$2s^22p^53p\ ^3P_1$	69.1003	69.1570	69.0003	68.9678	69.0941
14	$2s^22p^53p\ ^1D_2$	69.1402	69.2008	69.0411	69.0097	69.1369
15	$2s^22p^53p\ ^1S_0$	70.0837	70.2499	70.1372	70.1203	70.0599
16	$2s^22p^53d\ ^3P_0$	71.0603	71.1264	70.9484	70.9199	71.0761
17	$2s^22p^53d\ ^3P_1$	71.1490	71.2239	71.0377	71.0093	71.1644
18	$2s^22p^53d\ ^3P_2$	71.3137	71.4019	71.2055	71.1776	71.3240
19	$2s^22p^53d\ ^3F_4$	71.3092	71.4096	71.2029	71.1752	71.3248
20	$2s^22p^53d\ ^3F_3$	71.3607	71.4437	71.2575	71.2340	71.3676
21	$2s^22p^53d\ ^1D_2$	71.5080	71.5928	71.4098	71.3861	71.4998
22	$2s^22p^53d\ ^3D_3$	71.6041	71.7083	71.5079	71.4847	71.5973
23	$2s^22p^53d\ ^3D_1$	72.0028	72.1387	71.9452	71.9256	72.0192
24	$2s^22p^53d\ ^3F_2$	72.6505	72.7348	72.5485	72.5263	72.6617
25	$2s^22p^53d\ ^3D_2$	72.7265	72.8272	72.6191	72.6005	72.7346
26	$2s^22p^53d\ ^1F_3$	72.7796	72.8836	72.6726	72.6564	72.7920
27	$2s^22p^53d\ ^1P_1$	73.2823	73.4547	73.2548	73.2464	73.3387
28	$2s2p^63s\ ^3S_1$	76.1637	76.0905	75.9685	75.9179	76.0394
29	$2s2p^63s\ ^1S_0$	76.6922	76.6420	76.5136	76.4612	76.5453
30	$2s2p^63p\ ^3P_0$		78.8035	78.6856	78.6288	78.7562
31	$2s2p^63p\ ^3P_1$	78.5640	78.8478	78.7275	78.6701	78.7972
32	$2s2p^63p\ ^3P_2$		79.1025	78.9785	78.9231	79.0459
33	$2s2p^63p\ ^1P_1$	78.9731	79.2543	79.1374	79.0767	79.1836
34	$2s2p^63d\ ^3D_1$		82.5614	82.4049	82.3630	82.5247
35	$2s2p^63d\ ^3D_2$		82.5888	82.4203	82.3787	82.5451
36	$2s2p^63d\ ^3D_3$		82.6376	82.4501	82.4089	82.5807
37	$2s2p^63d\ ^1D_2$		83.0283	82.8611	82.8349	82.9545
38	$2s^22p^54s\ ^3P_2$		87.4340	87.2557	87.1882	87.3495
39	$2s^22p^54s\ ^1P_1$	87.3449	87.4794	87.3103	87.2418	87.3995
40	$2s^22p^54p\ ^3S_1$		88.4761	88.3083	88.2410	88.4117
41	$2s^22p^54p\ ^3D_2$		88.5396	88.3755	88.3064	88.4710
42	$2s^22p^54p\ ^3D_3$		88.6148	88.4565	88.3882	88.5530
43	$2s^22p^54p\ ^1P_1$		88.6414	88.4864	88.4172	88.5784
44	$2s^22p^54p\ ^3P_2$		88.6935	88.5414	88.4719	88.6285
45	$2s^22p^54s\ ^3P_0$		88.7381	88.5592	88.4959	88.6644
46	$2s^22p^54s\ ^3P_1$	88.6207	88.7610	88.5863	88.5223	88.6908
47	$2s^22p^54p\ ^3P_0$		89.0180	88.8778	88.8116	88.9147
48	$2s^22p^54p\ ^3D_1$		89.8241	89.6556	89.5915	89.7666
49	$2s^22p^54d\ ^3P_0$		89.8633	89.6923	89.6308	89.8053
50	$2s^22p^54d\ ^3P_1$	89.7142	89.9037	89.7307	89.6695	89.8418
51	$2s^22p^54p\ ^3P_1$		89.9367	89.7797	89.7152	89.8858
52	$2s^22p^54p\ ^1D_2$		89.9566	89.7997	89.7347	89.9049
53	$2s^22p^54d\ ^3F_4$	89.8783	89.9595	89.7800	89.7186	89.8919
54	$2s^22p^54d\ ^3F_3$	89.8974	89.9696	89.7988	89.7381	89.9055
55	$2s^22p^54d\ ^3P_2$		89.9698	89.7945	89.7335	89.9028
56	$2s^22p^54d\ ^1D_2$		90.0223	89.8526	89.7923	89.9538
57	$2s^22p^54d\ ^3D_3$		90.0641	89.8883	89.8282	89.9894
58	$2s^22p^54p\ ^1S_0$		90.1459	90.0186	89.9571	90.0498
59	$2s^22p^54d\ ^1P_1$	90.1334	90.2812	90.1093	90.0559	90.1881
60	$2s^22p^54f\ ^3D_1$		90.6112	90.4620	90.3808	90.5167

Notes. [a] Sources of the NIST v3 are from the work of Sugar & Corliss (1985) and references therein. [b] GRASP data are from the work of Aggarwal & Keenan (2006). [(c)] Data in CHIANTI are from the work of Zhang et al. (1987).

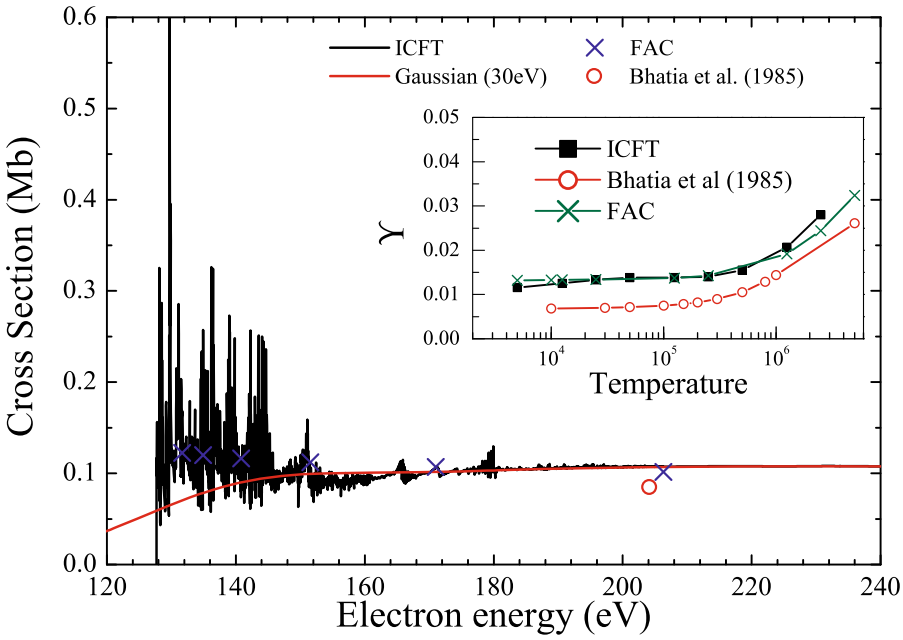

Fig. 2. Comparison of the collision cross-section and ϒ of Si^{4+} for $2s^22p^6\ ^1S_0 \rightarrow 2s^22p^53d\ ^3D_1$ (3*D*) excitation between the present ICFT *R*-matrix and previous calculations. Red smooth solid line is Gaussian convolution with width of 30 eV. [*Colour online*]

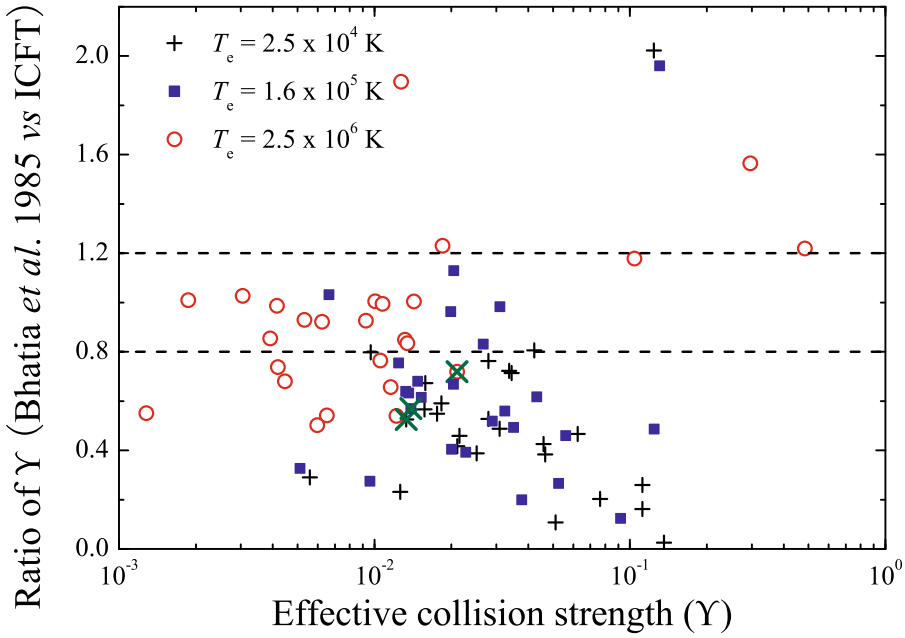

Fig. 3. An extensive comparison (all available excitations from the ground state) of effective collision strength ϒ for Si^{4+} between the present ICFT *R*-matrix and previous available data (DW calculation of Bhatia et al. (1985), from CHIANTI v6.0 database) at low (2.5×10^4 K), intermediate (1.6×10^5 K, that of peak fraction in ionization equilibrium) and high (2.5×10^6 K) temperatures. Horizontal dashed lines denote agreement of 20%. "×" symbols correspond to the 3*D* transition in Fig. 2. [*Colour online*]

due to the limited number of resonances included in their isolated resonant approximation, viz., autoionizing levels from the following configurations: $2s^22p^6n_2l_2$, $2s^22p^53ln_3l_3$, $2s^22p^64ln_4l_4$ with $n_{2,3} \leq 45$, $n_4 \leq 10$, $l_2 \leq 9$, $l_3 \leq 7$, and $l_4 \leq 4$ included, see Landi & Gu (2006). At the high temperature, 91% of transitions are within 20% in the comparison between the ICFT and Dirac *R*-matrix calculations. The comparison with data of Landi & Gu (2006) shows that the percentage is up to 60%-a value comparable to the structure assessment. At the intermediate temperature of 4.0×10^6 K with peak fractional abundance in ionization equilibrium (Mazzotta et al. 1998; Bryans et al. 2006), the percentage is 55% and 88% when compared with data of Landi & Gu (2006) and Loch et al. (2006), respectively. This is within the range defined by the above mentioned extreme cases (low and high temperatures), being close to the case of the high temperature. In other words, the resonance enhancement on the ϒ has significantly decreased at the temperature of the peak fractional abundance in the ionization equilibrium. The differences at lower temperatures suggests that caution should be exercised when using data from the isolated resonance approximation for high-precision spectroscopic modelling of astrophysical and laboratory plasmas.

— Kr^{26+} Griffin et al. (2008) performed a 139-level *R*-matrix calculations using the Dirac method. Two separate calculations were done: one with radiation damping and one without. Figure 7 shows the cross-section (original and a Gaussian convolution with a width of 30 eV) and a comparison of ϒ between our present ICFT *R*-matrix result and that of Griffin et al. (2008). Our original and convoluted cross-section show good agreement with data of Griffin et al. (2008), see Fig. 2-c in their work. The

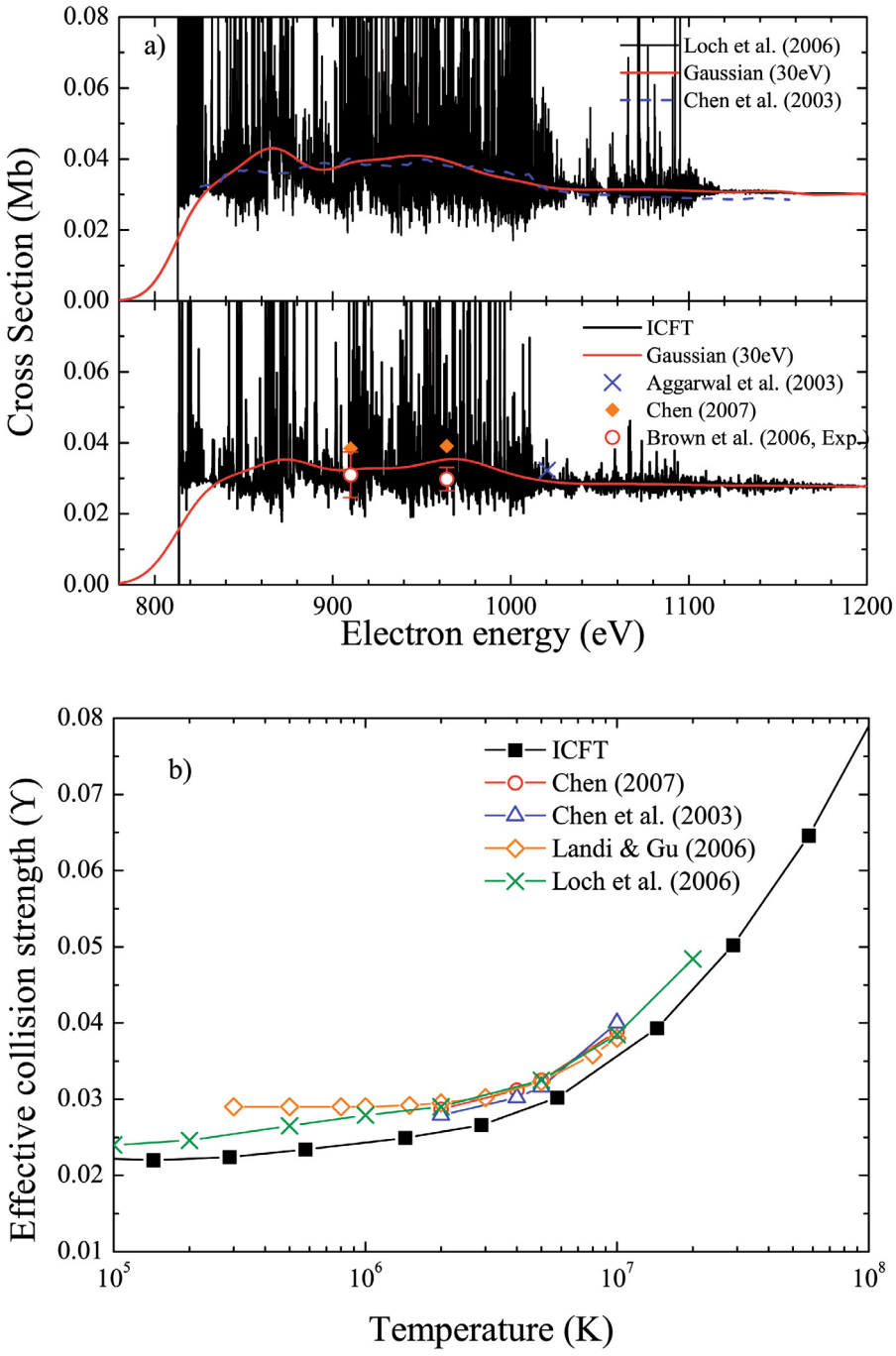

Fig. 4. Comparison of the collision cross-section and ϒ of Fe^{16+} for $2s^22p^6\ {}^1S_0 \rightarrow 2s^22p^53d\ {}^3D_1$ ($3D$) excitation between the present ICFT R-matrix and previous calculations. **a)** *Top*: the result of Loch et al. (2006) who used a finer energy mesh (around 10 times) than present calculation. The smooth-lines are cross-sections convoluted by Gaussian with a width of 30 eV (solid: Loch et al. 2006; dashed: Chen et al. 2003). *Bottom*: the present ICFT R-matrix result along with Gaussian convolution (the width of 30 eV) and previous Dirac R-matrix calculations (Chen 2007, Gaussian convolution; Aggarwal et al. 2003, unconvoluted), as well as experimental measurements of Brown et al. (2006) at two energies. **b)** The effective collision strength ϒ from different R-matrix calculations, and the DW plus isolated resonance approximation employed by Landi & Gu (2006). [*Colour online*]

background agrees well with the DW calculation from Bhatia et al. (1985) – see the point at E_e = 1904.8 eV. The 27-level ($2s^22p^6$ and $2s^22p^53l$) BPRM calculation of Gupta et al. (2000) has no resonances above E_e = 2000 eV. Strong resonances attached to the $2s2p^63l$ and $2s^22p^54l$ configurations appear, as demonstrated in the work of Griffin et al. (2008). The cross-section at E_e = 2040.9 eV (derived by us from the collision strength given at E_e = 150 Ryd) of Gupta et al. (2000) agrees well with the background of present ICFT R-matrix calculation. The present resultant ϒ is also consistent with the data of Griffin et al. (2008) both with and without radiative damping, being within 3% over the entire temperature range. Good agreement is also found when compared with Gupta et al.'s data.

Since a complete dataset of ϒ of Dirac R-matrix data (Griffin et al. 2008) is available from the CFADC[7], we make an extensive comparison of ϒ between the two different R-matrix datasets for Kr^{26+}, as shown in Fig. 8. At the low temperature $T_e = 5.0 \times 10^6$ K, 75% of excitations from ground state show agreement of 20%. The percentage increases up to 88% at the high temperature of $T_e = 5.0 \times 10^7$ K.

Griffin et al. (2008) made a statistical analysis of ϒ over temperatures from $T_e = 5.0 \times 10^6$ K to $T_e = 5.0 \times 10^7$ K for 9591 transitions among 139 levels, and found the average difference between the ϒ with and without damping to be 1.58%. As we know, radiative rates have a dependence of q^4 (where q is residual charge) for $\delta n > 0$ transitions. In their Na-like iso-electronic

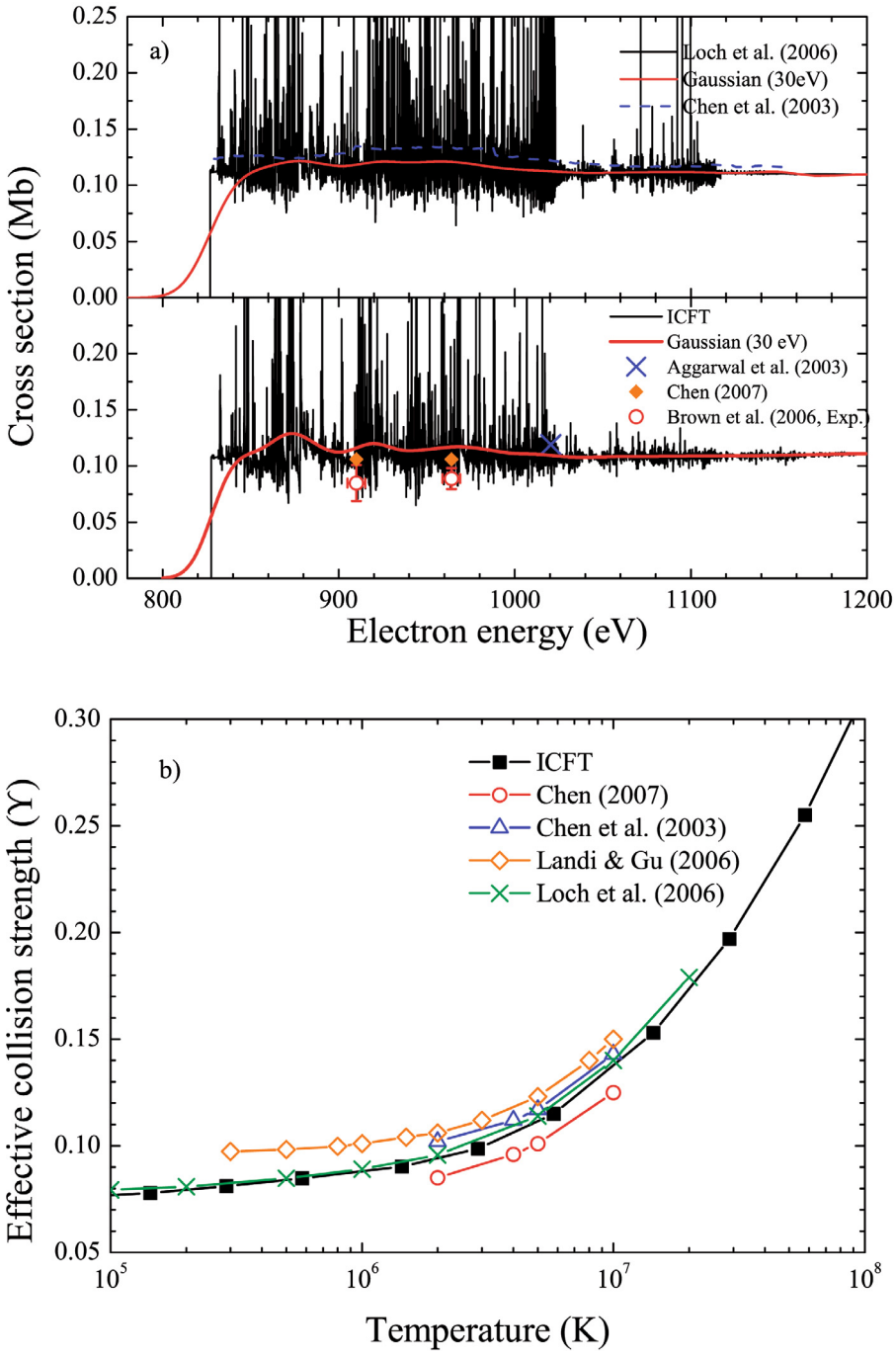

Fig. 5. Comparison of the collision cross-section and Υ of Fe^{16+} for $2s^22p^6\ ^1S_0 \rightarrow 2s^22p^53d\ ^1P_1$ (3*C*) excitation between the present ICFT *R*-matrix and previous calculations. The same figure caption as in Fig. 4. [*Colour online*]

sequence *R*-matrix calculation, Liang et al. (2009b) tested that the radiative damping becomes dominant with increasing of ionic charge. So, the radiative damping effect for the present ions of the Ne-like iso-electronic sequence will be negligible. The present ICFT *R*-matrix calculations without radiative damping are accurate over the sequence in this respect.

From the above comparison for the three specified ions (Si^{4+}, Fe^{16+} and Kr^{26+}) spanning the sequence, we believe that the present ICFT *R*-matrix results (σ and Υ) have the comparable level of accuracy with other *R*-matrix calculations, including both Dirac and Breit-Pauli *R*-matrix methods. Except for Fe, Ni and Kr, the present results are the only *R*-matrix ones, to-date. For ions near neutral (below Si^{4+}), *R*-matrix with pseudostates calculations are likely needed to model ionization loss, but the present are the best data available, to-date.

4.2. Iso-electronic trends of Υs

As noted in the work of Witthoeft et al. (2007), the level mixing effect for higher excited levels strongly affects the behaviour of the Υ along the sequence. Similar level-ordering cross was identified by Liang et al. (2009b) in *R*-matrix EIE calculation of Na-like iso-electronic sequence. Witthoeft & Badnell (2008) and Liang et al. (2009b) noticed that taking configuration, total angular momentum *J* and energy ordering as good quantum number is a better choice for level matching in comparison between two different calculations and investigation of Υ

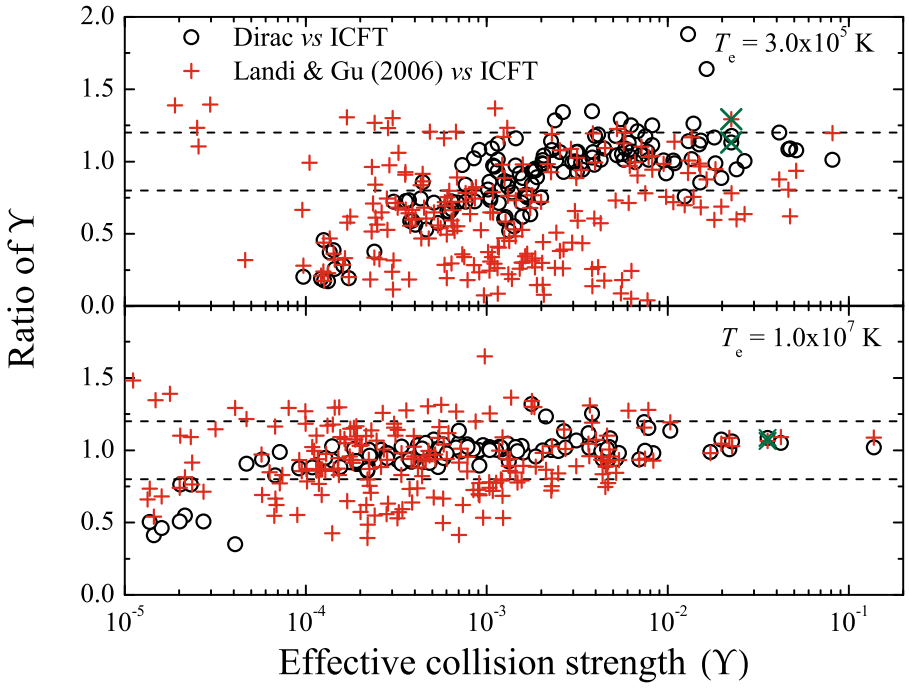

Fig. 6. An extensive comparison (all excitations from the ground state) of effective collision strength Υ of Fe^{16+} between the present ICFT *R*-matrix and Dirac *R*-matrix (Loch et al. 2006)[7] calculations, as well as results of Landi & Gu (2006) using an isolated resonance approximation, at low (3.0×10^5 K) and high (1.0×10^7 K) temperatures. Horizontal dashed lines denote agreement of 20%. "×" symbols correspond to the 3*D* transition in Fig. 4. [*Colour online*]

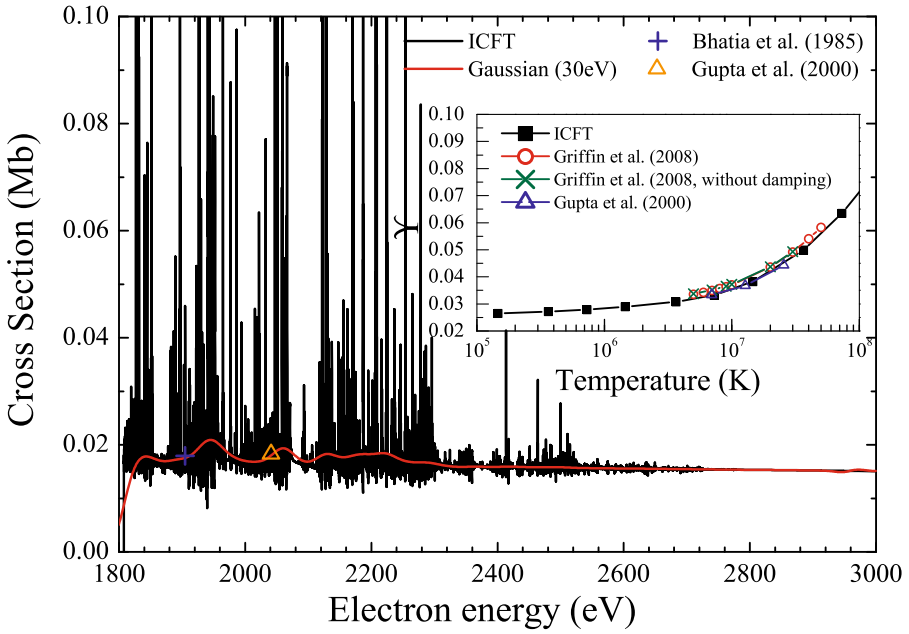

Fig. 7. Comparison of the collision cross-section and Υ of Kr^{26+} for $2s^22p^6$ $J = 0 \rightarrow 2s^22p^53d$ $J = 1$ (3*D*) excitation between the present ICFT *R*-matrix and previous calculations including Dirac *R*-matrix results of Griffin et al. (2008) with and without radiative damping, Breit-Pauli *R*-matrix results of Gupta et al. (2000) and DW cross-sections of Bhatia et al. (1985) at E_e = 1904.8 eV. Red smooth solid line is Gaussian convolution with width of 30 eV. [*Colour online*]

along the iso-electronic sequence. We find this to be true again, and map all ions relative to the level ordering of Fe^{16+} in the following discussion, see Fig. 9. This satisfactorily eliminates uncertainty originating from the non-continuity of level-ordering along the sequence. The choice of reference ion, Fe here, is of course irrelevant.

In Fig. 10, we show effective collision strength Υ at $T_e = 10^3(q+1)^2$, $10^4(q+1)^2$ and $10^5(q+1)^2$ K along the sequence for four dominant and strong transition lines in Ne-like ions: $2s^22p^53s\,^3P_1(3G)$, $^1P_1(3F) \rightarrow 2s^22p^6\,^1S_0$ (see Fig. 10a) and $2s^22p^53d\,^1P_1(3C)$ and $^3D_1(3D) \rightarrow 2s^22p^6\,^1S_0$ (see Fig. 10b). At the low temperature of $10^3(q+1)^2$ K, spikes and/or dips are observed along the sequence for the 3s → 2p transitions. However, there are no clear spikes and/or dips for 3d → 2p transitions. As pointed out by Witthoeft et al. (2007), such spikes/dips along the iso-electronic sequence at low temperature are due to the steady shifting of groups of resonances. This indirectly indicates that resonances are more important for the 3s → 2p transitions than for the 3d → 2p transitions. With increasing temperature, the spikes and/or dips disappear, as expected, because the resonance contribution becomes weaker and eventually negligible. For the 3*D* transition line, the Υ increases again below $Z = 15$ at the high temperature of $10^5(q+1)^2$ K. This is due to the high-energy collision strengths that are proportional to $gf/\Delta E$, as discussed for Si^{4+} for this transition line.

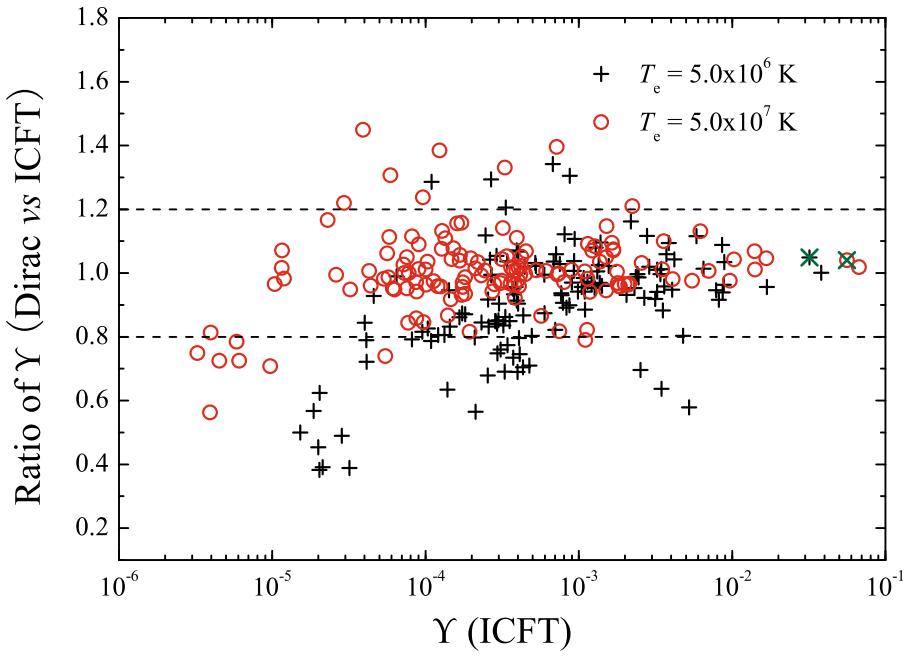

Fig. 8. An extensive comparison (all excitations from the ground state) of effective collision strength Υ for Kr^{26+} between the present ICFT *R*-matrix and Dirac *R*-matrix (Griffin et al. 2008)[7] calculations at low (5.0×10^6 K) and high (5.0×10^7 K) temperatures. Horizontal dashed lines denote agreement of 20%. "×" symbols correspond to the 3*D* transition in Fig. 7. [*Colour online*]

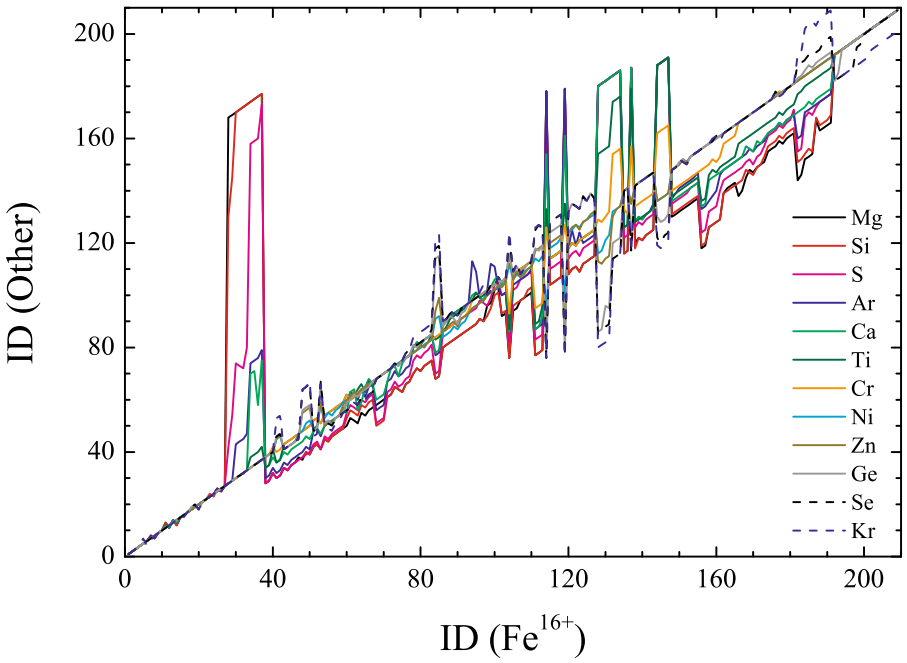

Fig. 9. The level ordering with the original level index (ID) relative to the ordering of Fe^{16+} by mapping according to the good quantum number – configuration, total angular momentum *J* and energy ordering for ions spanning the entire sequence. The spikes and dips are due to the shift of a given level, for example, $2s2p^6 3l$ (28–37) levels in Fe^{16+} move to levels above 120 in Si^{4+}. [*Colour online*]

5. Summary

We have performed 209-level ICFT *R*-matrix calculations of electron impact excitations with extensive configuration interaction (1337 LS terms or 2775 fine-structure levels) for all ions of the Ne-like iso-electronic sequence from Na^+ to Kr^{26+}. The present work is the most extensive and complete *R*-matrix data for modelling, to-date.

Good agreement with the available NIST v3 experimentally derived or CHIANTI v6 observed data and the results of others for level energies and gf-values for six specific ions (Si^{4+}, Ar^{8+}, Ca^{10+}, Fe^{16+}, Ni^{18+} and Kr^{26+}) spanning the iso-electronic sequence supports the reliability of the present *R*-matrix excitation data. This was confirmed specifically, by detailed comparisons of Ω/σ and Υ for Si^{4+}, Fe^{16+} and Kr^{26+}.

The comparison (in the cases of Fe^{16+} and Kr^{26+}) with calculations using fully relativistic Dirac *R*-matrix method reveals that present excitation data from ICFT *R*-matrix shows the same level of accuracy. Excellent agreement of atomic structure for lower charged ions, e.g. Si^{4+}, gives us insight that the present excitation data is better than previous data (from the DW approximation) extensively used by the astrophysical and spectroscopic communities. It is noted that the isolated resonance approach appears to underestimate the resonant enhancement of Υ for the majority of excitations in the case of Fe^{16+}.

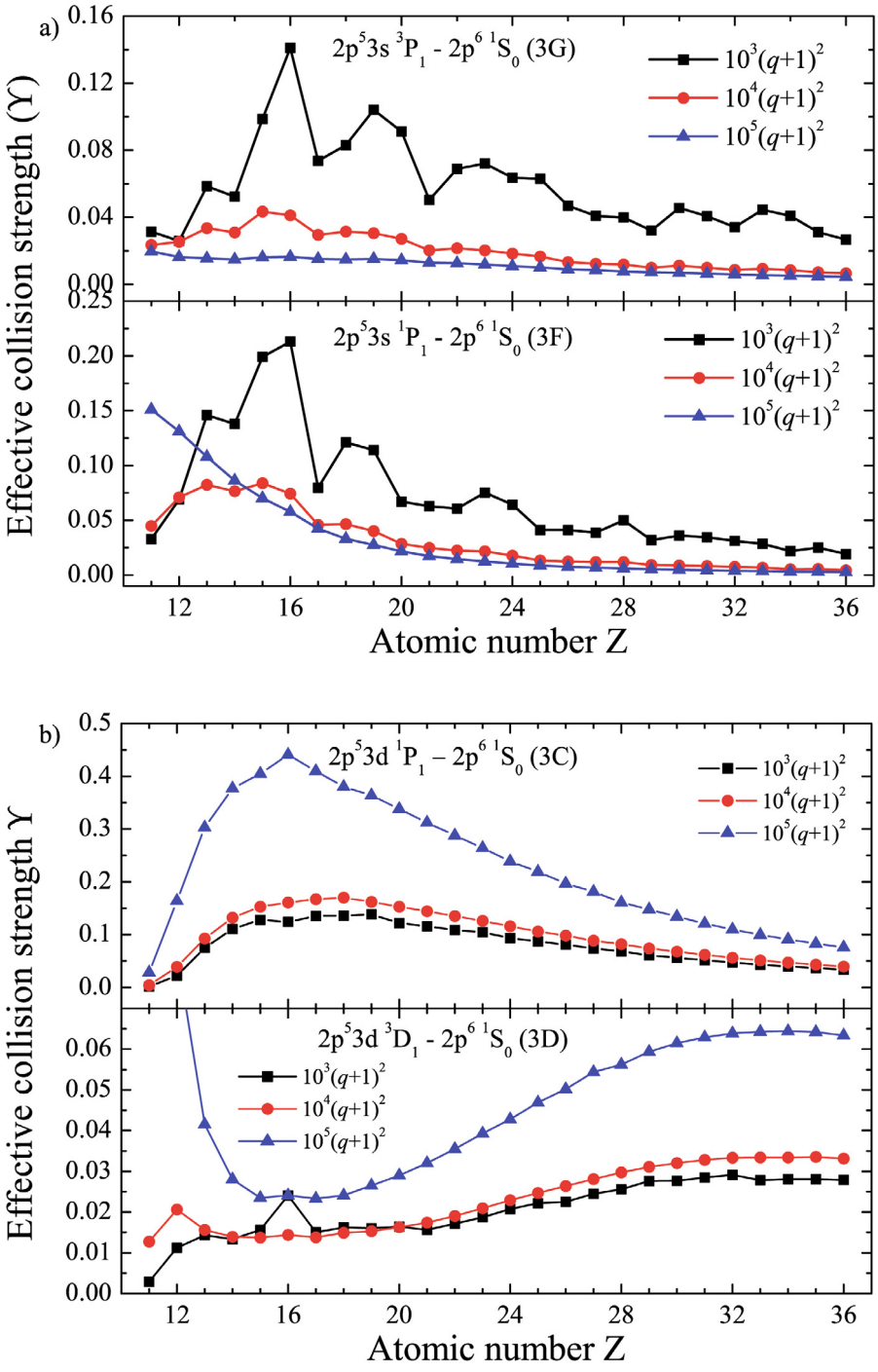

Fig. 10. Effective collision strength (Υ) at temperatures of $T_e = 10^{3,4,5}(q+1)^2$ K (here $q = Z - 10$) along the iso-electronic sequence. **a)** $2s^2 2p^5 3s\ ^3P_1(3G)$ and $^1P_1(3F) \rightarrow 2s^2 2p^6\ ^1S_0$ transitions; **b)** $2s^2 2p^5 3d\ ^1P_1(3C)$ and $^3D_1(3D) \rightarrow 2s^2 2p^6\ ^1S_0$ transitions. [*Colour online*]

By excluding the level crossing effects on the Υ, we examined the iso-electronic trends of the effective collision strengths. A complicated pattern of spikes and dips of Υ at low temperatures was noted again along the sequence, which precludes interpolation in Z. With increasing temperature, the difference between the present ICFT R-matrix and previous DW results decreases as expected.

The data are made available through archives of the APAP website 1 in the ADAS adf04 format (Summers 2004), OPEN-ADAS 3 and CHIANTI[8].

In conclusion, we have generated an extensive set of reliable excitation data utilizing the ICFT R-matrix method for spectroscopy/diagnostic research within the astrophysical and fusion communities. This will replace data from DW and isolated resonance approaches presently used by these communities, for most ions, and its use can be expected to identify new lines and may overcome some shortcomings in present astrophysical modelling, as seen previously for Mg^{8+} (Del Zanna 2008), Fe^{6+} and Fe^{7+} (Del Zanna 2009a,b), and Si^{9+} (Liang et al. 2009c).

[8] http://www.chianti.rl.ac.uk/

Table 11. Comparison of the weighted oscillator strength gf between the AS and other calculations for Ni^{18+}.

$i-j$	AS		MCDF[a]	CHIANTI[b]	FAC
	gf_L	gf_V/gf_L			
1–3	1.29^{-1}[c]	0.90		1.16^{-1}	1.29^{-1}
1–5	9.39^{-2}	0.97	9.93^{-2}	9.13^{-2}	1.01^{-1}
1–17	8.86^{-3}	0.98	1.02^{-2}	1.00^{-2}	1.02^{-2}
1–23	7.93^{-1}	0.99	8.19^{-1}	8.51^{-1}	8.12^{-1}
1–27	2.35^{+0}	1.00	2.46^{+0}	2.55^{+0}	2.33^{+0}
1–31	4.69^{-2}	1.01	4.71^{-2}	5.30^{-2}	4.70^{-2}
1–33	2.98^{-1}	1.05	2.90^{-1}	3.51^{-1}	2.99^{-1}
1–39	2.32^{-2}	0.79	2.65^{-2}	2.57^{-2}	2.42^{-2}
1–46	1.46^{-2}	0.93	1.88^{-2}	1.78^{-2}	1.73^{-2}
1–50	3.05^{-3}	0.95	3.56^{-3}	3.10^{-3}	3.54^{-3}
1–59	4.04^{-1}	0.96	4.47^{-1}	3.78^{-1}	4.12^{-1}
1–71	3.92^{-1}	0.97	4.63^{-1}	3.67^{-1}	4.04^{-1}
2–6	2.46^{-1}	1.24	2.48^{-1}	2.31^{-1}	2.44^{-1}
2–7	2.37^{-1}	1.08	2.43^{-1}	2.40^{-1}	2.38^{-1}
2–8	7.62^{-1}	0.99	7.74^{-1}	7.49^{-1}	7.61^{-1}
2–9	9.26^{-3}	0.98	9.37^{-3}	1.05^{-2}	9.18^{-3}
2–10	3.24^{-1}	0.94	3.28^{-1}	3.22^{-1}	3.23^{-1}
2–14	3.47^{-3}	0.72	3.56^{-3}	3.53^{-3}	3.48^{-3}
2–28	3.19^{-1}	0.40	3.33^{-1}	3.28^{-1}	3.30^{-1}
2–40	2.56^{-1}	0.96	2.56^{-1}	2.40^{-1}	2.62^{-1}
2–41	2.01^{-1}	0.96	2.05^{-1}		2.11^{-1}
2–44	2.12^{-1}	1.00	2.04^{-1}	1.95^{-1}	2.09^{-1}
3–7	2.59^{-1}	1.16	2.59^{-1}	2.50^{-1}	2.54^{-1}
3–9	3.07^{-1}	1.10	3.11^{-1}	3.01^{-1}	3.05^{-1}
3–10	2.63^{-1}	0.97	2.71^{-1}	2.65^{-1}	2.65^{-1}
3–11	1.00^{-1}	0.89	1.02^{-1}	1.01^{-1}	1.01^{-1}
3–15	6.88^{-2}	0.72	7.08^{-2}	7.20^{-2}	6.82^{-2}
3–28	8.12^{-2}	0.41	8.60^{-2}	8.49^{-2}	8.60^{-2}
3–29	7.35^{-2}	0.30	7.70^{-2}	7.57^{-2}	7.35^{-2}
3–41	2.46^{-1}	0.94	2.43^{-1}		2.48^{-1}
3–43	2.52^{-1}	0.95	2.54^{-1}	2.41^{-1}	2.56^{-1}
3–44	1.88^{-1}	0.98	1.91^{-1}	1.83^{-1}	1.94^{-1}
3–47	7.04^{-2}	1.02	7.00^{-2}	6.71^{-2}	6.99^{-2}
4–6	1.16^{-3}	2.56	1.16^{-3}		1.15^{-3}
4–12	1.12^{-1}	1.11	1.13^{-1}	1.12^{-1}	1.11^{-1}
4–13	2.04^{-1}	0.97	2.08^{-1}	2.03^{-1}	2.04^{-1}
4–28	5.91^{-2}	0.51	6.08^{-2}	6.11^{-2}	6.03^{-2}
4–48	9.27^{-2}	0.94	9.27^{-2}	8.71^{-2}	9.53^{-2}
4–51	1.60^{-1}	0.99	1.57^{-1}	1.50^{-1}	1.62^{-1}
5–11	2.44^{-2}	1.20	2.46^{-2}	2.53^{-2}	2.33^{-2}
5–12	1.78^{-1}	1.19	1.79^{-1}	1.74^{-1}	1.76^{-1}
5–13	1.13^{-1}	1.04	1.15^{-1}	1.12^{-1}	1.13^{-1}
5–14	5.51^{-1}	1.01	5.60^{-1}	5.43^{-1}	5.49^{-1}
5–15	1.20^{-1}	0.84	1.25^{-1}	1.32^{-1}	1.24^{-1}
5–29	4.79^{-2}	0.38	4.94^{-2}	5.06^{-2}	4.77^{-2}
5–48	1.77^{-1}	0.94	1.78^{-1}	1.67^{-1}	1.81^{-1}
5–51	8.28^{-2}	0.98	8.29^{-2}	7.94^{-2}	8.38^{-2}
5–58	7.48^{-2}	1.00	7.45^{-2}	7.00^{-2}	7.43^{-2}

Notes. Index number corresponds to that in Table 10. [(a)] GRASP data are from the work of Aggarwal & Keenan (2006). [(b)] Data in CHIANTI are from the work of Zhang et al. (1987). [(c)] x^y denotes $x \times 10^y$.

Table 12. The level energies (Ryd) of Kr^{26+} from different calculations along with the compilation of NIST v3.

ID	Level specification	NIST[a]	AS	FAC	MCDF[b]
1	$2s^22p^6\ ^1S_0$		0.000		
2	$2s^22p^53s\ ^3P_2$	121.204	121.384	121.242	121.192
3	$2s^22p^53s\ ^1P_1$	121.441	121.592	121.482	121.426
4	$2s^22p^53p\ ^3S_1$	124.966	125.274	125.019	124.964
5	$2s^22p^53s\ ^3P_0$	125.284	125.452	125.283	125.303
6	$2s^22p^53p\ ^3D_2$	125.194	125.503	125.250	125.200
7	$2s^22p^53s\ ^3P_1$	125.399	125.562	125.406	125.430
8	$2s^22p^53p\ ^3D_3$	126.041	126.352	126.097	126.072
9	$2s^22p^53p\ ^1P_1$	126.084	126.370	126.136	126.100
10	$2s^22p^53p\ ^3P_2$	126.397	126.686	126.449	126.410
11	$2s^22p^53p\ ^3P_0$	127.618	127.907	127.633	127.588
12	$2s^22p^53p\ ^3D_1$	129.175	129.491	129.194	129.225
13	$2s^22p^53p\ ^3P_1$	130.192	130.485	130.208	130.241
14	$2s^22p^53p\ ^1D_2$	130.280	130.582	130.302	130.347
15	$2s^22p^53d\ ^3P_0$	130.694	131.065	130.788	130.745
16	$2s^22p^53p\ ^1S_0$	130.742	131.105	130.936	130.908
17	$2s^22p^53d\ ^3P_1$	130.945	131.257	130.961	130.936
18	$2s^22p^53d\ ^3F_3$	131.173	131.523	131.236	131.232
19	$2s^22p^53d\ ^3P_2$	131.233	131.589	131.282	131.266
20	$2s^22p^53d\ ^3F_4$	131.214	131.622	131.267	131.274
21	$2s^22p^53d\ ^1D_2$	131.445	131.803	131.510	131.496
22	$2s^22p^53d\ ^3D_3$	131.664	132.059	131.728	131.723
23	$2s^22p^53d\ ^3D_1$	132.476	132.866	132.553	132.551
24	$2s^22p^53d\ ^3F_2$	135.260	135.550	135.239	135.304
25	$2s^22p^53d\ ^3D_2$	135.426	135.816	135.458	135.522
26	$2s^22p^53d\ ^1F_3$	135.531	135.929	135.567	135.640
27	$2s^22p^53d\ ^1P_1$	136.065	136.470	136.152	136.226
28	$2s2p^63s\ ^3S_1$		139.301	138.999	139.030
29	$2s2p^63s\ ^1S_0$		140.228	139.784	139.808
30	$2s2p^63p\ ^3P_0$		143.315	142.899	142.923
31	$2s2p^63p\ ^3P_1$	142.715	143.393	142.973	143.005
32	$2s2p^63p\ ^3P_2$		144.298	143.888	143.939
33	$2s2p^63p\ ^1P_1$	143.835	144.486	144.090	144.137
34	$2s2p^63d\ ^3D_1$		149.200	148.746	148.814
35	$2s2p^63d\ ^3D_2$		149.283	148.804	148.884
36	$2s2p^63d\ ^3D_3$		149.470	148.935	149.027
37	$2s2p^63d\ ^1D_2$	149.295	150.012	149.526	149.623
38	$2s^22p^54s\ ^3P_2$		164.741	164.395	164.361
39	$2s^22p^54s\ ^1P_1$	164.388	164.798	164.476	164.439
40	$2s^22p^54p\ ^3S_1$		166.296	165.965	165.929
41	$2s^22p^54p\ ^3D_2$		166.352	166.029	165.992
42	$2s^22p^54p\ ^3D_3$		166.663	166.375	166.350
43	$2s^22p^54p\ ^1P_1$		166.670	166.396	166.367
44	$2s^22p^54p\ ^3P_2$		166.771	166.503	166.469
45	$2s^22p^54p\ ^1S_0$		167.275	167.045	166.996
46	$2s^22p^54d\ ^3P_0$		168.441	168.136	168.116
47	$2s^22p^54d\ ^3P_1$	168.120	168.512	168.204	168.190
48	$2s^22p^54d\ ^3F_3$		168.591	168.295	168.284
49	$2s^22p^54d\ ^3D_2$		168.629	168.324	168.310
50	$2s^22p^54d\ ^3F_4$		168.644	168.319	168.314
51	$2s^22p^54d\ ^1D_2$		168.699	168.401	168.388
52	$2s^22p^54d\ ^3D_3$		168.793	168.484	168.473
53	$2s^22p^54s\ ^3P_0$		168.824	168.451	168.493
54	$2s^22p^54s\ ^3P_1$	168.376	168.833	168.470	168.510
55	$2s^22p^54d\ ^1P_1$	168.738	169.136	168.851	168.844
56	$2s^22p^54f\ ^3D_1$		169.620	169.348	169.319
57	$2s^22p^54f\ ^1G_4$		169.649	169.370	169.350
58	$2s^22p^54f\ ^3D_2$		169.661	169.386	169.359
59	$2s^22p^54f\ ^3G_5$		169.697	169.397	169.377
60	$2s^22p^54f\ ^3F_3$		169.711	169.440	169.414

Notes. [a] Sources of the NIST v3 compilation are from the work of Saloman (2007) and references therein. [(b)] MCDF data is from the work of Griffin et al. (2008).

Table 13. Comparison of the weighted oscillator strength gf between the AS and other calculations for Kr^{26+}.

$i-j$	AS		MCDF[a]	RFG00[b]	ZSC87[c]
	gf_L	gf_V/gf_L			
1–3	1.34^{-1}[d]	0.83	1.34^{-1}		1.34^{-1}
1–7	7.86^{-2}	0.96	8.45^{-2}		8.45^{-2}
1–17	4.45^{-3}	0.96	6.41^{-3}	7.79^{-3}	6.00^{-3}
1–23	1.53^{+0}	1.00	1.55^{+0}	1.54^{+0}	1.55^{+0}
1–27	1.90^{+0}	1.00	1.93^{+0}	1.94^{+0}	2.09^{+0}
1–31	8.90^{-2}	1.01	8.97^{-2}	8.75^{-2}	9.70^{-2}
1–33	3.12^{-1}	1.06	3.05^{-1}	3.05^{-1}	3.78^{-1}
1–39	2.38^{-2}	0.69	2.48^{-2}	2.47^{-2}	2.30^{-2}
1–47	2.44^{-3}	0.93	3.26^{-3}		3.90^{-2}
1–54	6.88^{-2}	0.95	7.94^{-2}	6.80^{-2}	5.00^{-3}
1–55	4.20^{-1}	0.97	4.29^{-1}	4.34^{-2}	4.12^{-1}
1–71	3.15^{-1}	0.99	3.38^{-1}	3.30^{-1}	3.11^{-1}
1–79	2.19^{-2}	0.69	2.97^{-2}	3.33^{-2}	
1–81	2.15^{-2}	0.98	1.77^{-2}	1.30^{-2}	
1–83	1.17^{-1}	0.96	1.20^{-1}	1.17^{-1}	
1–97	2.03^{-1}	0.95	2.24^{-1}	2.33^{-1}	
1–123	1.58^{-3}	0.91	2.50^{-3}		
1–131	1.11^{-1}	0.99	1.31^{-1}	1.37^{-1}	

Notes. Index number corresponds to that in Table 12. [(a)] Corresponds to the work of Griffin et al. (2008). [(b)] RFG00 refers to the calculation of Rice et al. (2000). [(c)] ZSC87 refers to the calculation of Zhang et al. (1987). [(d)] x^y denotes $x \times 10^y$.

Table 14. The energy meshes (in unit of q^2, residual charge of ion) used for each ion.

mesh	Atomic number			
q^2Ryd	11–14	15–17	18–30	31–36
1×10^{-4}	•			
5×10^{-5}		•		
1×10^{-5}			•	
5×10^{-6}				•

Acknowledgements. The work of the UK APAP Network is funded by the UK STFC under grant no. PP/E001254/1 with the University of Strathclyde. G.Y.L. thanks H. E. Mason, G. Del Zanna, P. J. Storey and K. A. Berrington for some helpful discussions.

References

Aggarwal, K. M., Keenan, F. P., & Msezane, A. Z. 2003, ApJS, 144, 169
Aggarwal, K. M., & Keenan, F. P. 2006, A&A, 460, 959
Aggarwal, K. M., & Keenan, F. P. 2008, A&A, 488, 365
Badnell, N. R. 1986, J. Phys. B: At. Mol. Opt. Phys., 19, 3827
Badnell, N. R., & Griffin, D. C. 1999, J. Phys. B: At. Mol. Opt. Phys., 32, 2267
Badnell, N. R., & Griffin, D. C. 2001, J. Phys. B: At. Mol. Opt. Phys., 34, 681
Beiersdorfer, P., Behar, E., Boyce, K. R., et al. 2002, ApJ, 576, L169
Beiersdorfer, P., Goeler, S. V., Bitter, M., & Thorn, D. B. 2001, Phys. Rev. A, 64, 032705
Berrington, K. A., Eissner, W., & Norrington, P. H. 1995, Comput. Phys. Commun., 92, 290
Berrington, K. A., Ballance, C. P., Griffin, D. C., & Badnell, N. R. 2005, J. Phys. B: At. Mol. Opt. Phys., 38, 1667
Bhatia, A. K., Feldman, U., & Seely, J. F. 1985, At. Data Nucl. Data Tables, 32, 435
Brown, G. V., Beiersdorfer, P., Chen, H., et al. 2006, Phys. Rev. Lett., 96, 253201
Bryans, P., Badnell, N. R., Gorczyca, T. W., et al. 2006, ApJ, 691, 1540
Bryans, P., Landi, E., & Savin, D. W. 2009, ApJS, 167, 343
Burgess, A. 1974, J. Phys. B: At. Mol. Opt. Phys., 7, L364
Burgess, A., & Tully, J. A. 1991, A&A, 254, 436
Chen, G. X. 2007, Phys. Rev. A, 76, 062708
Chen, G. X. 2008, MNRAS, 386, L62
Chen, G. X., Pradhan, A. K., & Eissner, W. 2003, J. Phys. B: At. Mol. Opt. Phys., 36, 453
Chen, G. X., Kirby, K., Silver, E., et al. 2006, Phys. Rev. Lett., 97, 143201
Del Zanna, G. 2009a, A&A, 508, 501
Del Zanna, G. 2009b, A&A, 508, 513
Del Zanna, G., & Ishikawa, Y. 2009, A&A, 508, 1517
Del Zanna, G., Rozum, I., & Badnell, N. R. 2008, A&A, 487, 1203
Dere, K. P., Landi, E., Young, P. R., et al. 2009, A&A, 498, 915
Fournier, K. B., & Hansen, S. B. 2005, Phys. Rev. A, 71, 012717
Griffin, D. C., Badnell, N. R., & Pindzola, M. S. 1998, J. Phys. B: At. Mol. Opt. Phys., 31, 3713
Griffin, D. C., Ballance, C. P., Mitnik, D. M., & Berengut, J. C. 2008, J. Phys. B: At. Mol. Opt. Phys., 41, 215201
Gu, M. F. 2008, Can. J. Phys., 86, 675
Gu, M. F., Beiersdorfer, P., Brown, G. V., et al. 2004, ApJ, 607, L143
Gupta, G. P., Deb, N. C., & Msezane, A. Z. 2000, Phys. Scr., 61, 175
Hummer, D. G., Berrington, K. A., Eissner, W., et al. 1993, A&A, 279, 298
Landi, E., & Gu, M. F. 2006, ApJ, 640, 1171
Lepson, J. K., Beiersdorfer, P., Behar, E., & Kahn, S. M. 2003, ApJ, 590, 604
Liang, G. Y., Whiteford, A. D., & Badnell, N. R. 2008, J. Phys. B: At. Mol. Opt. Phys., 41, 235203
Liang, G. Y., Whiteford, A. D., & Badnell, N. R. 2009a, A&A, 500, 1263
Liang, G. Y., Whiteford, A. D., & Badnell, N. R. 2009b, J. Phys. B: At. Mol. Opt. Phys., 42, 225002
Liang, G. Y., Whiteford, A. D., & Badnell, N. R. 2009c, A&A, 499, 943
Loch, S. D., Pindzola, M. S., Ballance, C. P., & Griffin, D. C. 2006, J. Phys. B: At. Mol. Opt. Phys., 39, 85
Martin, W. C., & Zalubas, R. 1983, J. Phys. Chem. Ref. Data, 12, 323
Mathews, D. L., Hagelstein, P. L., Rosen, M. D., et al. 1985, Phys. Rev. Lett., 54, 110
Mazzotta, P., Mazzitelli, G., Colafrancesco, S., & Vittorio, N. 1998, A&AS, 133, 403
Norrington, P. H., & Grant, I. P. 1987, J. Phys. B: At. Mol. Opt. Phys., 20, 4869
Rice, J. E., Fournier, K. B., Goetz, J. A., Marmar, E. S., & Terry, J. L. 2000, J. Phys. B: At. Mol. Opt. Phys., 33, 5435
Saloman, E. B. 2007, J. Phys. Chem. Ref. Data, 36, 215
Shirai, T., Sugar, J., & Musgrove, A. 1999, unpublished, see http://physics.nist.gov/PhysRefData/ASD/Html/ref.html#Kelly
Smith, B. W., Raymond, J. C., & Mann, J. B. 1985, ApJ, 298, 898
Sugar, J., & Corliss, C. 1985, in Atomic Energy Levels of the Iron Period Elements Potassium Through Nickel, 14, Suppl. 2
Summers, H. P. 2004, The ADAS User manual version 2.6 http://www.adas.ac.uk/
Tomasel, F. G., Rocca, J. J., Shlyaptsev, V. N., & Macchietto, C. D. 1997, Phys. Rev. A, 55, 1437
Zhang, H. L., Sampson, D. H., Clark, R. E. H., & Mann, J. B. 1987, At. Data Nucl. Data Tables, 37, 17
Witthoeft, M. C., Whiteford, A. D., & Badnell, N. R. 2007, J. Phys. B: At. Mol. Opt. Phys., 40, 2969
Witthoeft, M. C., & Badnell, N. R. 2008, A&A, 481, 543